

Molecular-exciton approach to spin-charge crossovers in dimerized Hubbard and excitonic chains

D. Mukhopadhyay

Department of Chemistry, Princeton University, Princeton, New Jersey 08544

G. W. Hayden

Department of Physics and Earth Sciences, Mercer University, Macon, Georgia 31207

Z. G. Soos

Department of Chemistry, Princeton University, Princeton, New Jersey 08544

(Received 17 October 1994; revised manuscript received 22 December 1994)

The crossover from band to correlated states in half-filled quantum cell models is studied in a molecular-exciton framework based on a chain of dimers. Crystal states with one or several excited dimers yield analytical excitation energies to first order in interdimer Coulomb interactions $V(p,p')$ for excitonic chains or interdimer electron transfer $t_- = t(1-\delta)$ for Hubbard chains. Molecular-exciton analysis of excitations and transition moments rationalizes exact numerical solutions of oligomers with arbitrary intradimer correlations U , V_1 , and electron transfer $t_+ = t(1+\delta)$, including the number, positions, and transition moments of low-lying excitations. Short correlation lengths of infinite chains with large alternation $\delta \geq 0.6$ lead to converged crystal states for oligomers containing $N=4-7$ dimers. The present approach provides a detailed picture of excited-state crossovers with increasing U , V_1 , and $V(p,p')$. Quite generally, the lowest singlet excitation S_1 is one-photon allowed ($1B$) on the band side of the spin-charge crossover and two-photon allowed ($2A$) on the correlated side. Intermediate correlations and large δ reveal different crossovers in Hubbard chains, where $1B$ involves charge transfer between dimers, and excitonic chains, where $1B$ has an excited dimer. We also obtain two-photon transition moments M and extend vanishing $M(2A)$ in the band limit up to $U=2t_+$, the $\delta \sim 1$ crossover of Hubbard chains. We find finite $M(2A)$ on the correlated side, however, where $2A$ contains two triplet dimers in either alternating Hubbard or excitonic chains. Their different spin-charge crossovers appear as an abrupt and continuous increase, respectively, of two-photon intensity on going from the correlated to the band side. The greater delocalization ($\delta \sim 0.07-0.33$) realized in conjugate polymers is consistent with excitonic chains. The potential $V(p,p')$ in the Pariser-Parr-Pople model for conjugated hydrocarbons distinguishes strongly fluorescent polymers with $S_1=1B$ from others with $S_1=2A$. We also relate our results at large δ to other approximations for nonlinear optical spectra of conjugated polymers.

I. INTRODUCTION

Many recent studies¹⁻³ have explored the nonlinear optical (NLO) properties and electroluminescence (EL) of conjugated polymers in connection with a variety of applications. Pristine polymers are semiconductors with optical gaps around 2-3 eV whose electronic excitations are the microscopic basis for NLO responses and EL. The Su-Schrieffer-Heeger (SSH) model⁴ describes the coupling between electronic states and lattice vibrations for noninteracting π electrons in a Hückel or tight-binding chain. The low-lying excitations are solitons and polarons for polymers with a degenerate ground state, such as *trans*-polyacetylene (PA), and bipolarons for many other polymers with nondegenerate ground states. These self-localized states have been widely applied⁵ to polymer spectra generated by chemical doping or photoexcitation. Quantum fluctuations of the lattice strongly enhance⁶ the NLO response of *trans*-PA over that of *cis*-PA. The neutral excitations⁷ of conjugated polymers and hydrocarbons also indicate the importance of electron-electron ($e-e$) correlations, notably through exciton formation in polydiacetylenes, negative spin densities in PA, and different energy thresholds⁸ for triplet, one-photon, two-photon, and charge-carrying excitations. Since NLO

coefficients are formally given⁹ as sums over virtual states and their transition dipoles, correlations rather than excited-state relaxation are probed. The lowest singlet excitation S_1 is dipole allowed in conjugated polymers that fluoresce strongly, but two-photon allowed in systems with weak or extrinsic emission.¹⁰ Increasing $e-e$ correlations ensure¹¹ a sharp S_1 crossover from dipole to two-photon allowed in centrosymmetric polymers.

Many-body and exciton theories are traditional approaches to $e-e$ correlations in extended systems, especially for ground states and energy thresholds, and some exact results are known for uniform Hubbard, Heisenberg, or related chains with one orbital or spin per site.^{7,12} Alternating single and double bonds in the PA ground state preclude exact analysis for interacting π electrons. Electronic states of extended systems such as conjugated polymers have consequently been approximated by a variety of techniques for both π - and all-electron models.^{5,2} Our discussion of correlated states is restricted to quantum cell models with one orbital per site. In contrast to direct solution of many-electron problems, exciton theories¹³ for organic crystals such as anthracene start with molecular excitations observed in the gas phase and apply degenerate perturbation theory to the intermolecular interactions and lower symmetry in the solid. Crystal states

then implicitly contain molecular correlations.

The PA backbone in Fig. 1, with two sites per unit cell, has generally been used for modeling the half-filled π systems of conjugated polymers. Alternating transfer integrals $t_{\pm} = t(1 \pm \delta)$ lead to an energy gap $4t\delta$ between the filled valence and empty conduction bands in the noninteracting limit. We introduce an arbitrary spin-independent potential $V(p, p')$ and consider the evolution of the ground and excited states. On-site repulsions $U \gg t$ in Hubbard models lead to localized spins with antiferromagnetic Heisenberg exchange $J \sim 2t^2/U$, and such spin-charge separation is typical for any $V(p, p')$ that favors uniform charge distribution in the ground state. Mott's analysis¹⁴ of the metal-insulator transition of atomic hydrogen invokes variable bandwidth $4t$ in a uniform ($\delta=0$) lattice. The hypothetical variation of $4t$ in dimerized chains produces a crossover between localized spins for $U \gg t$ and a semiconductor for $t \gg U$. Since the symmetry of S_1 is different in the two limits, the crossover¹¹ can be precisely associated with the symmetry change. Spin-charge crossovers naturally occur at intermediate correlations $U \sim 2t$ realized in conjugated polymers.⁷ We expect similar correlations $V(p, p')$ in conjugated backbones of sp^2 - or sp -hybridized carbon atoms. Different bond lengths, topologies, and substituents modulate the observed optical gaps and can be modeled¹⁰ in terms of the PA backbone with variable δ at fixed bandwidth $4t$ and correlations $V(p, p')$. The present study is motivated by the generality of spin-charge crossovers in quantum cell models and the realization of conjugated polymers on either side.

Intermediate correlations $U \sim 2t$ are particularly challenging. Band theories with $U=0$ are highly developed and have recently been extended¹⁵⁻¹⁷ to include Coulomb interactions between an electron in the conduction band and hole in the valence band. Corrections for weak $e-e$ correlations suggest configuration-interaction (CI) schemes,^{18,19} but CI in extended systems is not size consistent²⁰ beyond the first order, and that is not sufficient for intermediate correlations. Strong correlations $U \gg t$ have also been treated rigorously in terms of Heisenberg spin chains in half-filled systems^{21,12} or t - J models for other filling.²² Degenerate perturbation theory generates²³ corrections in $(t/U)^{2n}$. None of these methods extend to intermediate correlations, which is precisely the relevant regime for the spin-charge crossover. The lack of accurate solutions at intermediate correlations has led to controversies²⁴ about correlated states of simple extended systems. One issue is the location and NLO contributions of even-parity states below the lowest one-

photon absorption; another is the role of biexcitons above the one-photon transition involving two-electron excitations in the band limit. Lattices with uniform t 's have attracted most theoretical attention. They illustrate maximum delocalization and avoid such chemical details as bond-length variations in conjugated polymers. To obtain correlated states in the crossover region of extended systems, we consider below chains in the opposite limit of reduced delocalization and start with dimers whose correlated states are exactly known for arbitrary U/t .

We develop in this paper a general approach to excited states of infinite chains with intermediate correlations and focus on the spin-charge crossover where S_1 switches from a dipole-allowed to a two-photon excitation. We obtain analytical solutions in Sec. II for a chain of isolated dimers, or molecules, that correspond in Fig. 1 to a C=C bond with transfer integrals $t_+ = t(1 + \delta)$. Electron transfer and Coulomb interactions between dimers are treated analytically by first-order perturbation theory for the infinite chain and verified by exact numerical solutions to oligomers. The single bond $t_- = t(1 - \delta)$ in Fig. 1 is a sufficiently small perturbation for $\delta \geq 0.6$ to demonstrate convergence for 14-site oligomers. Such large alternation δ is not directly applicable to conjugated polymers, which are more extensively delocalized. But the polysilane backbone with $\delta = \frac{1}{3}$ provided initial applications²⁵ of dimer states, and the direct characterization of crystal states and transition moments²⁶ allows us to follow all low-energy excitations through the spin-charge crossover. Moreover, since the unit cell in Fig. 1 is the same for any $\delta > 0$, the state symmetries also hold for alternations realized in conjugated polymers.

Our approach is a generalization of molecular-exciton theory.¹³ We find dimer states explicitly and consider parameter regimes in which dimer excitations cross. Electron transfer or $e-e$ interactions between dimers mix the states too strongly to use perturbation theory. We then resort to exact analysis of oligomers with sufficiently large δ to ensure convergence to the infinite chain. Exact solutions to quantum cell models with one orbital per site take advantage of the large but finite basis for oligomers.²⁷ Diagrammatic valence bond (VB) methods²⁸ are convenient for any model that conserves the total spin S and yield transition dipoles and NLO coefficients²⁹ as well as excitation energies. Oligomers up to 14 sites are currently feasible. Whether this suffices for infinite chains depends on the electron coherence length, which in the noninteracting limit³⁰ involves the ratio of the bandwidth $4t$ and band gap $4t\delta$. The coherence length is clearly a unit cell for decoupled dimers ($\delta=1$) and diverges for regular ($\delta=0$) chains. We combine analytical dimer and exciton functions for infinite chains with exact oligomer results to follow all excitations in the crossover region. We can thereby distinguish between different parameter regimes of Hubbard, extended Hubbard, or Pariser-Parr-Pople (PPP) models.

The PA backbone in Fig. 1 illustrates the partitioning used throughout this paper. We consider transfer integrals $t(1 \pm \delta)$ along a chain of $2N$ sites, with sites $2p, 2p - 1$ corresponding to the p th dimer, and arbitrary spin-independent interactions $V(p, p')$ between electrons

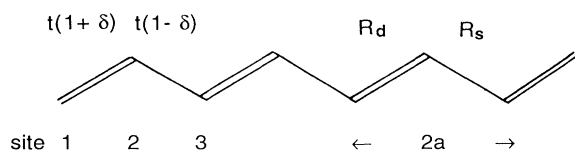


FIG. 1. Partial single and double bonds of *trans*-polyacetylene, with unit cell $2a$, transfer integrals $t(1 \pm \delta)$, bond lengths $R_s = 1.45 \text{ \AA}$, $R_d = 1.35 \text{ \AA}$, and bond angles $2\pi/3$.

on sites p, p' . The half-filled case has one electron per site, two per dimer. The π -electron Hamiltonian is

$$H(\delta) = H_d(\delta) + H_-(\delta) + V_{dd}, \quad (1)$$

where H_d is restricted to one dimer, H_- transfers electrons between dimers, and V_{dd} contains all interdimer $V(p, p')$ interactions. Similar H_d occur in all half-filled dimers,

$$H_d = t_+ \sum_{p\sigma} (a_{2p\sigma}^\dagger a_{2p-1\sigma} + a_{2p-1\sigma}^\dagger a_{2p\sigma}) + U_e \sum_p n_p(n_p - 1)/2, \quad (2)$$

with $t_+ = t(1 + \delta)$, $U_e = U - V(R_d)$ for bond length R_d in Fig. 1, and π -electron number operators n_p . The dimer states form a complete basis for (1). Interdimer contributions are restricted to electron transfer $t_- = t(1 - \delta)$ in Hubbard models and also include Coulomb interactions in excitonic models,

$$H_-(\delta) = t(1 - \delta) \sum_p (a_{2p\sigma}^\dagger a_{2p+1\sigma} + a_{2p+1\sigma}^\dagger a_{2p\sigma}), \quad (3)$$

$$V_{dd} = +\frac{1}{2} \sum_{pp'} V(R_{pp'}) q_p q_{p'},$$

where $q_p = 1 - n_p$ is the π -electron charge operator and the primed sum is restricted to p, p' in different dimers. The form of $V(p, p') = V(|p' - p|)$ is arbitrary at this stage and depends on the distances $R_{pp'}$ between sites in Fig. 1. Large alternation δ and interdimer separations $R_{pp'}$ clearly reduce (3) to a small perturbation. The excited states of (1) are accessible in this regime and can be followed with increasing interdimer coupling.

The paper is organized as follows. We introduce dimer states in Sec. II, construct crystal states with one or several excited dimers, and obtain approximate analytical solutions in the dimer ($\delta=1$) limit. The major distinction is between systems whose lowest dipole-allowed singlet is a band state or an exciton. We then demonstrate in Sec. III convergence for threshold excitations of $2N=14$ chains with $\delta=0.6$, compare one- and two-photon excitations of oligomers with crystal energies in the crossover region, and relate $\delta=0.6$ eigenstates of oligomers to the dimer basis. We present in Sec. IV transition dipoles for one- and two-photon excitations of linear oligomers due to mixing of dimer states by $H_-(\delta)$ and discuss the different behavior for two-photon intensities of band and excitonic systems at the S_1 crossover. We then discuss correlated spectra of (1) and comment on previous applications of Hubbard and PPP models to NLO spectra or photophysics of conjugated polymers.

II. MOLECULAR-EXCITON THEORY NEAR THE DIMER LIMIT

Conjugated polymers often have centrosymmetric backbones in their idealized extended conformation. Dipole-allowed transitions to odd-parity states and two-photon transitions to even-parity states then follow by

symmetry. The C_{2v} backbone in Fig. 1 has even-parity A_g singlets, including the ground state $|G\rangle$, and odd-parity B_u singlets. Thus S_1 is either 2^1A_g or 1^1B_u , taken as $2A$ and $1B$ below. We invoke the usual⁷ π -electron or tight-binding restrictions to one orbital per site, nearest-neighbor hopping integrals $t_{p,p+1}$, and the zero-differential-overlap (ZDO) approximation³¹ for $e-e$ interactions, which restricts $V(p, p')$ to two-center integrals. Half-filled models (1) with arbitrary spin-independent $e-e$ interactions also have^{32,33} electron-hole ($e-h$) or charge-conjugation symmetry. We choose $e-h$ index $J=1$ for $|G\rangle$. Two-photon excitations conserve J , while dipole transitions reverse J . Translational symmetry for $2N$ sites gives crystal states with wave vector $k = \pi m/Na$ and $-\pi/2 < k \leq \pi/2$ in the first Brillouin zone. The many-electron states of (1) have fixed, J , k , and total spin S . The ZDO approximation for the dipole operator μ is

$$\mu = \sum_p e r_p q_p. \quad (4)$$

We suppose the alternating chains (1) to be along the z axis and consider dipole processes polarized along the chain; transverse components can be treated the same way. All NLO coefficients⁹ reduce to matrix elements of (4) in the dipole approximation and $k=0$ singlets with $J = \pm 1$ are sufficient in general for (1).

Electron transfer between dimers generates ion radicals $D^+\sigma$ or $D^-\sigma$. Solution of (2) is again elementary, since the cation and anion have one electron and one hole, respectively, but Coulomb interactions between charged dimers n, n' are potentially large. We incorporate first-order corrections $\langle V_{dd} \rangle$ in the zeroth-order Hamiltonian

$$H_0 = H_d + \frac{1}{2} \sum_{pp'} V(R_{pp'}). \quad (5)$$

We take all expectation values with respect to the eigenstates of H_d and note that H_0 conserves the electron count $n_{2p} + n_{2p-1}$ separately for each dimer. The perturbations (3) then become $H_-(\delta)$ and $\Delta V_{dd} = V_{dd} - \langle V_{dd} \rangle$. The H_0 spectrum is restricted to dimers and reduces to H_d excitations in the limit of isolated dimers.

Figure 2 shows the excitations and eigenstates of a neutral dimer,³⁴ whose second-quantized eigenstates are explicitly given in Appendix A and are simply the H_2 functions with CI in the $1s$ orbitals. The triplet $|t\rangle$ has parallel spins on both sites and is strictly covalent, with $n_p \equiv 1$, while the ionic singlet $|b\rangle$ is the odd linear combination of both electrons on the same site. The ground state $|g\rangle$ and excited state $|a\rangle$ are even-parity singlets whose composition depends on U_e/t_+ . For $U_e \gg t_+$, $|g\rangle$ is the covalent (Heitler-London) singlet with one electron per site and $|a\rangle$ is the ionic, even linear combination of both electrons on the same site. Intradimer correlations are governed by the mixing of $|g\rangle$ and $|a\rangle$ according to

$$\tan 2\varphi = 4t_+/U_e. \quad (6)$$

There is equal mixing in the Hückel ($U_e=0$) limit. As indicated in Fig. 2, we reference all excitation energies to

$$\begin{array}{l}
|a\rangle \text{ ---} \\
|b\rangle \text{ ---} \\
|t\rangle \text{ ---} \\
|g\rangle \text{ ---}
\end{array}
\begin{array}{l}
|a\rangle = \sin\phi|-\rangle - \cos\phi(|+-\rangle + |-+\rangle)/\sqrt{2} \\
\varepsilon_a = \sqrt{U_e^2 + 16t_+^2} = 2\varepsilon_t + U_e \\
|b\rangle = (|+-\rangle - |-+\rangle)/\sqrt{2} \\
\varepsilon_b = (\sqrt{U_e^2 + 16t_+^2} + U_e)/2 = \varepsilon_t + U_e \\
|t\rangle = |-\rangle \\
\varepsilon_t = (\sqrt{U_e^2 + 16t_+^2} - U_e)/2 \\
|g\rangle = \cos\phi|-\rangle + \sin\phi(|+-\rangle + |-+\rangle)/\sqrt{2}
\end{array}$$

FIG. 2. Excitation energies and eigenfunctions of H_d , Eq. (2), for a neutral dimer with mixing angle $2\varphi = \tan^{-1}4t_+/U_e$ in Eq. (6) between the even-parity covalent singlet $|-\rangle$ and ionic states $|+-\rangle$ and $|-+\rangle$. The triplet $|t\rangle$ has parallel spins denoted by an arrow, while the odd-parity singlet $|b\rangle$ is strictly ionic.

the ground state. We have

$$\varepsilon_t = (\sqrt{U_e^2 + 16t_+^2} - U_e)/2, \quad (7)$$

while $|b\rangle$ is at $\varepsilon_b = \varepsilon_t + U_e$ and $|a\rangle$ at $\varepsilon_a = 2\varepsilon_t + U_e$; $|b\rangle$ and $|a\rangle$ are one- and two-photon allowed, respectively, and the latter clearly corresponds to two-electron excitation in the Hückel limit. The dimer excitations are related by

$$\varepsilon_a = \varepsilon_b + \varepsilon_t. \quad (8)$$

As the triplet excitation (7) decreases with increasing U_e , $|a\rangle$ and $|b\rangle$ become degenerate to order t_+^2/U_e . The transition dipoles (4) between $|b\rangle$ and $|g\rangle$ or $|a\rangle$ are, respectively, $eR_d \sin\varphi$ and $eR_d \cos\varphi$, as can be verified using the functions in Appendix A.

The radical ions D^+ and D^- contain one electron and one hole, respectively. Their ground energies are $-|t_+|$ and $U - |t_+|$, with the full on-site repulsion in the anion and delocalization $-t_+$ of the electron in D^+ or hole in D^- . The CT singlet $|D_n^+ D_{n+r}^- \rangle$ with charged dimers at n and $n' = n + r$ is given in Appendix A. To construct eigenstates with $e-h$ symmetry, we combine states with reversed charges,

$$|CTn, r, \pm 1\rangle = (|D_n^+ D_{n+r}^- \rangle \pm |D_n^- D_{n+r}^+ \rangle) / \sqrt{2}. \quad (9)$$

They transform as $J = \pm 1$ for arbitrary separation $2ra$ between the charged dimers. First-order excitation energies for H_0 are

$$\begin{aligned}
E_{CT}(r) &= 2\varepsilon_t - 2t_+ + U - W(r), \\
W(r) &\equiv \{V(2n, 2n + 2r - 1) + 2V(2n, 2n + 2r) \\
&\quad + V(2n - 1, 2n + 2r)\} / 4.
\end{aligned} \quad (10)$$

The $W(r)$ contributions $\langle V_{dd} \rangle$ depend explicitly on the chain geometry in Fig. 1. In addition to singlet CT states (9), we have triplet CT states whose excitation energies

are also $E_{CT}(r)$ in first order. All CT states are degenerate in Hubbard chains, with $W(r) = 0$.

Crystal states are products of molecular functions, or of H_d eigenstates in the present context. The crystal ground state $|G\rangle = |gg \cdots g\rangle$ is nondegenerate, with $|g\rangle$ given by (A1) for arbitrary U_e/t_+ . Since $|g\rangle$ contains a pair of fermions, the ordering of the product is arbitrary and $|G\rangle$ is fully antisymmetric under electron interchange. The simplest crystal excitations contain one excited dimer. We define product functions $|T_n\rangle$, $|B_n\rangle$, and $|A_n\rangle$ to have a triplet, odd-parity, and even-parity excitation at dimer n and ground-state dimers elsewhere. Phases of the many-electron function are again independent of the ordering of operators in Appendix A. The normalized crystal states are

$$\begin{aligned}
|Tk\rangle &= N^{-1/2} \sum_n e^{i2ank} |T_n\rangle, \\
|Bk\rangle &= N^{-1/2} \sum_n e^{i2ank} |B_n\rangle, \\
|Ak\rangle &= N^{-1/2} \sum_n e^{i2ank} |A_n\rangle,
\end{aligned} \quad (11)$$

with $k = \pi m / Na$ in the first Brillouin zone. All N states in the triplet band have $S = 1$ and $J = 1$, while the entire $|Bk\rangle$ and $|Ak\rangle$ bands have $S = 0$, $J = -1$, and $S = 0$, $J = 1$, respectively.

Expectation values of H_0 in (5) with respect to (11) give first-order excitation energies. Neither $|T0\rangle$ nor $|A0\rangle$ is shifted by interdimer Coulomb interactions, since the operators q_p in V_{dd} connect³⁵ states with opposite J . The singlet-exciton band $|Bk\rangle$ is split, however, because $\langle B_p | q_p q_{p+1} | B_{p+1} \rangle$ does not vanish and the exciton can hop to a neighboring dimer. The first-order shift of $|B0\rangle$ is¹¹

$$\begin{aligned}
E_b^{(1)} &= -W_-(1 - \cos 2\varphi), \\
W_- &\equiv \{V(2n, 2n + 1) - 2V(2n, 2n + 2) \\
&\quad + V(2n - 1, 2n + 2)\}.
\end{aligned} \quad (12)$$

The shift is largest at $U_e = 0$ [$2\varphi = 0$ in (6)], when $|g\rangle$ is 50% ionic, and there is no shift at large U_e , when $|g\rangle$ is the covalent Heitler-London singlet. $|B0\rangle$ is at the bottom of the band in extended Hubbard models ($V_1 > 0$, $V_r = 0$, $r = 2, 3, \dots$), in PPP models ($V_1 - 2V_2 + V_3 > 0$), or any other $V(R)$ with positive curvature. The width of the exciton band is $2E_b^{(1)}$.

Molecular-exciton theories use crystal states (11) in systems whose excitation energies are large compared to intermolecular interactions. We focus instead on parameters in which the excitations of (1) are almost degenerate and also consider composite excitations in which two or more dimers are excited. States with two excited dimers resemble an electron-hole pair in band theory in having $\sim N$ states with $k = 0$ for the center of mass. Additional internal degrees of freedom lead to $\sim N^2$ and $\sim N^3$ states in the $k = 0$ manifolds for three and four excited dimers, respectively. The dimer basis provides controlled approximations at small t_- for enumerating all many-

electron excitations in subspaces with fixed S, J , and k .

We begin with triplet dimers at n and $n+r$ and obtain states with $J=1$ and $S=0, 1$, or 2 . The singlet combination $|TTn, r\rangle$ is given in Appendix A for any separation $2ar$. All TT states discussed below are $k=0$ singlets with $J=1$ and normalized wave functions

$$|TT_r\rangle = N^{-1/2} \sum_n |TTn, r\rangle, \quad r=1, 2, \dots, M, \quad (13)$$

with $M=N/2$ for even N and $(N-1)/2$ for odd N . The first-order energy is $2\epsilon_t$, independent of r or interdimer $e-e$ interactions. The TT states (13) are M -fold degenerate in the dimer limit and are all potentially two-photon active, but have vanishing intensities because $|t\rangle$ is purely covalent and thus does not couple to the dipole operator μ . Angular momentum addition leads to one singlet TTT state, while four triplets give two $TTTT$ singlets. The construction of crystal states with $k=0$ and excitation energy $p\epsilon_t$ is straightforward in either case.

The dimer basis also contains CT states whose long-range Coulomb interactions (10) are included in H_0 . The singlets $|CTn, r, \pm 1\rangle$ in (9) with charged dimers at n and $n+r$ generate a $k=0$ crystal state for each separation $2ar$,

$$|CT_r, \pm 1\rangle = N^{-1/2} \sum_n |CTn, r, \pm 1\rangle, \quad r=1, 2, \dots, M, \quad (14)$$

with excitation energy $E_{CT}(r)$ and $J=1$ or -1 . The potential $V(p, p')$ controls the spacing of the CT excitations. For completeness, we note that there are additional CT states in which one or both dimers are excited, either $2t_+$ or $4t_+$ higher in energy, and composite $k=0$ singlets based on $CT+T$, two CT pairs, doubly charged dimers, or other combinations of dimer excitations. Although elementary, the first-order spectrum of H_0 rapidly becomes congested with increasing energy and many different orderings of excited states are possible for various t_+ , U_e , and $V(p, p')$. Linear combinations of all these excitations appear automatically in exact analysis of oligomers.

Singlet excitons and composite TT or CT excitations exhaust the energy thresholds of H_0 . Intradimer correlations are fixed by (6), while interdimer $e-e$ interactions appear for CT states and for the singlet exciton $|B0\rangle$. The first-order excitation energies of these crystal states follow from (7), (8), (10), and (12),

$$\begin{aligned} E_{TT}/U_e &= 2\epsilon_t/U_e = (1 - \cos 2\varphi)/\cos 2\varphi, \\ E_b/U_e &= (1 + \cos 2\varphi)/2 \cos 2\varphi - W_- (1 - \cos 2\varphi)/U_e, \\ E_a/U_e &= 1/\cos 2\varphi, \end{aligned} \quad (15)$$

$$E_{CT}(r)/U_e = (2 - \sin 2\varphi)/2 \cos 2\varphi + [V(R_d) - W(r)]/U_e.$$

These analytical expressions hold for any spin-independent potential $V(p, p')$ in a chain with $t_- = 0$. The lowest dipole-allowed ($J=-1$) excitation is either the singlet exciton $|B0\rangle$ or a CT state, usually with adja-

cent D^+D^- , while the lowest $J=1$ singlet is either a TT or a CT state. The spin-charge crossover depends on the nature of the $J=-1$ threshold. We distinguish between excitonic chains with $E_b < E_{CT}(1)$ and ‘‘Hubbard’’ chains with the opposite ordering. The latter include extended Hubbard models with sufficiently small $V(p, p')$ to have $1B$ in the CT manifold at $t_- = 0$.

The energies (15) for excitonic chains are shown in Fig. 3, in units of E_b , as a function of intradimer correlations $2\varphi = \tan^{-1} 4t_+/U_e$. Solid and dashed lines correspond to $J=1$ and -1 , respectively, and the TT line is M -fold degenerate in the separation r . The actual curves are $k=0$ singlets for the Ohno potential³⁶

$$V(p, p') = V(R_{pp'}) = e^2/(\rho^2 + R_{pp'}^2)^{1/2}, \quad (16)$$

and the PA geometry in Fig. 1, with 120° bond angle and bond lengths $R_d = 1.35$ Å, $R_s = 1.45$ Å. The on-site repulsion $V(0) = e^2/\rho = 11.26$ eV for carbon is taken from atomic data and fixes the orbital size $\rho = 1.28$ Å. Although high-energy excitations in Fig. 3 depend on $V(R)$, the spin-charge crossover at $t_- = 0$ is fixed by the singlet exciton E_b . All spin states with $p \geq 2$ triplets have low energies $p\epsilon_t$ for $U_e \gg t_+$, while all CT states become degenerate on the t_+ scale for $t_+ \gg U_e$. For clarity, we have not shown all high-energy compound excitations in Fig. 3. The full spectrum of all k and S states is even more complicated, but is not needed for NLO spectra.

The $2A/1B$ crossover of excitonic chains is given by $E_{TT} = E_b$ in (15). This relates the triplet excitation at the crossover to the stabilization W_- :

$$\epsilon_t(W_-) = (U_e - 2W_- + \sqrt{9U_e^2 - 4U_e W_- + 4W_-^2})/4. \quad (17)$$

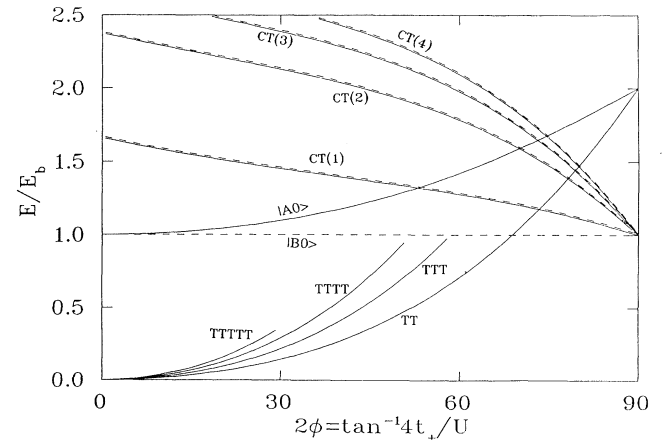


FIG. 3. Crystal excitations, Eq. (15), of excitonic chains in the dimer ($\delta=1$) limit as a function of intradimer correlations $2\varphi = \tan^{-1} 4t_+/U_e$, in units of E_b , to first order in the Ohno potential, Eq. (16), for the PA structure in Fig. 1. Solid and dashed lines are $k=0$ singlets with $J=1$ and -1 , respectively. The TT line is M -fold degenerate in the separation $2ar$ between triplets and some high-energy composite excitations have been omitted. The spin-charge crossover is between TT and $|B0\rangle$.

The $W_- = 0$ crossover of isolated dimers occurs at $U_e/t_+ = \sqrt{2}$. Since $W_- > 0$ lowers ϵ_t , the $2A/1B$ crossover shifts in Fig. 3 to higher $U_e/t_+ \sim 2$ for the Ohno potential. The dimer state $|A0\rangle$ at the crossover has $E_a/E_b = 1 + U_e/2\epsilon_t(W_-)$ and the ratio is 1.5 for $W_- = 0$. Two-electron excitation of the dimer is around $1.5E_b$ when S_1 becomes a TT state in chains with $\delta = 1$. Similar ratios occur in oligomers^{26,37} with the Ohno potential and smaller $\delta \sim 0.2$ where, however, the energy thresholds have not converged to the infinite chain. We note that TT and CT excitations cross in Fig. 3 at lower $U_e/4t_+$, with the first crossing for $E_{CT}(1)$. Since CT manifolds also contain $J=1$ states, the sharp TT/CT crossovers in Fig. 3 become avoided crossings for any $t_- \neq 0$ in (3) and these states are strongly mixed²⁵ at alternations realized in conjugated polymers.

The spin-charge crossover of Hubbard models is qualitatively different. All $V(p,p')$ vanish, U controls the intradimer correlations (6), and there are no potential terms in (15). The crossover of H_0 is now exactly at $U = 2t_+$ at $\delta = 1$ and involves TT and CT states because E_b is no longer the lowest $J = -1$ singlet. But the CT states (14) are split by $H_-(\delta)$ and are not proper zeroth-order states for $\delta < 1$. We again include first-order corrections in t_- for crystal excitations. The relevant matrix elements are¹¹

$$\langle CTr, J | H_-(\delta) | CTr', J' \rangle = t_- \sin 2\varphi \delta_{r,r\pm 1} \delta_{JJ'} \quad (18)$$

for CT states of either $e-h$ symmetry. Interdimer electron transfer connects $k=0$ singlets whose charge separation increases or decreases by $2a$. Since the CT states (14) are degenerate, (18) leads to a tridiagonal matrix with $r = 1, 2, \dots, M$ that maps into a regular Hückel chain with $t' = t_- \sin 2\varphi$. Hubbard chains with small t_- consequently form CT bands whose first-order corrections to E_{CT} in (15) are

$$e_p^{(1)} = -2|t_-| \sin 2\varphi \cos 2p\pi / (M+1), \quad p = 1, 2, \dots, M, \quad (19)$$

with $M = N/2$ for even N and $(N-1)/2$ for odd N . Since the entire band consists of $k=0$ singlets, the linear spectrum starts at $E(1B) = E_{CT} - 2t_- \sin 2\varphi$ and is symmetric about E_{CT} .

Figure 4 shows spin-charge crossovers in Hubbard chains with $\delta = 0.6$ ($t_-/t_+ = \frac{1}{4}$), in units of E_{CT} , as a function of intradimer correlations $2\varphi = \tan^{-1} 4t_+/U$. We again use solid lines for $k=0, J=1$ singlets, dashed lines for $k=0, J=-1$ singlets, and both for the CT band edges from (19). TT and TTT singlets appear at low energy on the correlated side and lead to additional compound excitations that are not shown in Fig. 4 for clarity. The singlet exciton E_b has higher energy. The crossover clearly involves a CT state for $1B$, but the lowest $J=1$ singlet is a mixture of TT and CT states for any $\delta < 1$. The mixing is necessarily strong because the crossing of $J=1$ states occurs at the same φ in first order.

Before comparing the analytical results in Figs. 3 and 4 for infinite chains with oligomer excitations, we summarize transition dipoles and the mixing of crystal states due

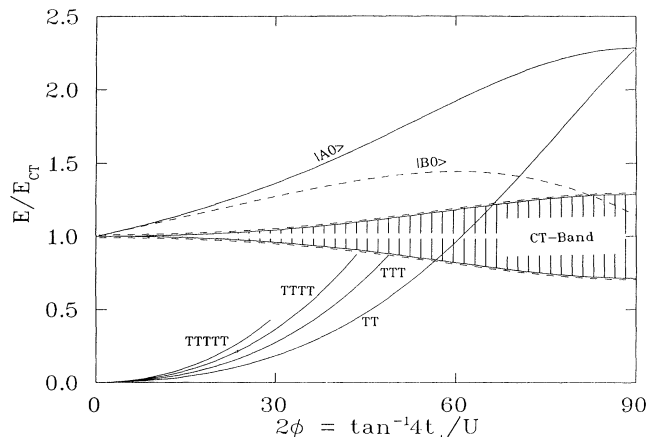


FIG. 4. Crystal excitations, Eq. (15), of Hubbard chains with $\delta = 0.6$ as a function of intradimer correlations $2\varphi = \tan^{-1} 4t_+/U$, in units of E_{CT} , to first order in interdimer hopping $H_-(\delta)$, Eq. (3). Solid and dashed lines are $k=0$ singlets with $J=1$ and -1 , respectively. The CT band is given by Eq. (19) and the TT line is M -fold degenerate. The spin-charge crossover is between TT and the edge of the CT band.

to $H_-(\delta)$. Only intradimer transitions in Fig. 2 are possible at $t_- = 0$, since the number of electrons on each dimer is conserved in H_0 . The crystal states (11), (13), or (14) are linear combinations of products of dimer states. Transition moments for singlet excitons (11) are

$$\mu_b = \langle Bk | \mu | G \rangle = N^{1/2} e R_d \sin \varphi \delta_{k,0}. \quad (20)$$

The intensity is entirely in the $k=0$ mode and μ_b^2 scales as the number of dimers N . The linear spectrum at $\delta = 1$ has a single line at E_b in (15), regardless of the location of CT states. The two-photon spectrum has a single line at E_a in the dimer limit. Using the transition dipole $e R_d \cos \varphi$ between $|B0\rangle$ and $|A0\rangle$ in (11), we obtain

$$M_a = \frac{\mu_a \mu_b}{E_b - E_a / 2} = N^{1/2} \frac{e^2 R_d^2 \sin 2\varphi}{2E_b - E_a} \quad (21)$$

for the two-photon transition moment. The intensity goes as M_a^2 and scales as N , as required on physical grounds for weakly coupled molecules. When $|g\rangle$ becomes covalent for $U_e \gg t_+$, φ is small and both the linear and two-photon intensities are weak.

Electron transfer between dimers has far more important consequences for transition dipoles than for excitation energies. Since all matrix elements of $H_0(\delta)$ over crystal states are found below, perturbation theory can be carried out formally to any order. The mixing of $|B0\rangle$ by $H_-(\delta)$ is exclusively to $|CT1, -1\rangle$ in the dimer basis. The matrix element is

$$\langle B0 | H_-(\delta) | CT1, -1 \rangle = t_- (\cos \varphi + \sin \varphi) / 2 \quad (22)$$

and depends on U_e/t_+ through (6). Small t_- shifts oscillator strength from $|B0\rangle$ to $|CT1, -1\rangle$, while the matrix element (18) insures smaller admixtures of CT states with $r > 1$. The magnitude of $W(r)$ in (10) governs the actual

mixing and thus depends on the potential $V(p,p')$. In Hubbard models, t_- generates the CT band (19) and $|CT1, -1\rangle$ now appears with coefficient c_{p1} in the p th eigenstate. We again use the connection between (18) and a regular Hückel chain to obtain a general expression³¹ for the coefficients

$$c_{pr} = [2/(M+1)]^{1/2} \sin p\pi r / (M+1), \quad p = 1, 2, \dots, M \quad (23)$$

of $k=0$ states $|CTr, -1\rangle$ with separation $2ar$ between charges. The oscillator strength borrowed from the exciton moment (20) is modulated as c_{p1}^2 over the symmetric CT band at E_{CT} . The maximum intensity is at the band center, $p = M/2 \sim N/4$, while the intensity at the band edges goes as M^{-1} . The red edge rapidly gains intensity, however, with increasing t_- and dominates the linear spectrum of linear conjugated systems.^{26,30} The admixture of $|CT1, 1\rangle$ in the CT band (19) with $J=1$ is also c_{p1} in (23).

The mixing of $J=1$ states by $H_-(\delta)$ is more diverse, with $|TT1\rangle$ and $|A0\rangle$ as well as $|CT1, 1\rangle$ appearing in lowest order. The matrix elements are

$$\begin{aligned} \langle TT1 | H_-(\delta) | CT1, 1 \rangle &= t_- , \\ \langle A0 | H_-(\delta) | CT1, 1 \rangle &= t_- (\sin 2\varphi + \cos 2\varphi) / 2 , \\ \langle G | H_-(\delta) | CT1, 1 \rangle &= N^{1/2} t_- (1 + \sin 2\varphi) / 2 . \end{aligned} \quad (24)$$

Different U_e/t_+ dependencies result from the different covalent and ionic compositions of dimer states, with $|t\rangle$ purely covalent, $|b\rangle$ purely ionic, and $|a\rangle$ mixed. When TT bands are lowest in Figs. 3 and 4, we expect $|TT1\rangle$ to be split off, or stabilized, by mixing with $|CT1, 1\rangle$; $2A$ then acquires two-photon intensity for finite t_- . Higher-order mixing couples in $|TTr\rangle$ states with $r > 1$, TTT states, and other composite states with $J=1$.

The admixture of CT states due to interdimer electron transfer generates many additional transition moments. For NLO coefficients in general, we also need transition dipoles between CT states with opposite $e-h$ symmetry:

$$\mu_{CT}(r) = \langle CTr, J | \mu | CTr', -J \rangle = 2ear\delta_{rr'} . \quad (25)$$

The orthonormality of the dimer states gives the restriction $r=r'$ and the unit cell $2a$ in Fig. 1 fixes the magnitude. Very large transition dipoles occur at large separation r between the charged dimers, but the matrix elements (22) and (24) show $r=1$ to be most important for excitations of $|G\rangle$. For completeness, we note that both transition dipoles and $H_-(\delta)$ matrix elements can readily be extended to composite excitations within the dimer basis. But spin-charge separation depends on low-lying states of H_d with one or two excited dimers. We turn next to oligomer calculations to test the rich variety of excitations and transition moments predicted near the dimer limit.

III. EXCITATION ENERGIES AND CORRELATED STATES OF CYCLIC OLIGOMERS

Molecular-exciton analysis of alternating chains (1) works best in the dimer limit, where it yields analytical

results for all excitations. The first-order contributions discussed above can be extended to second order, but rapidly become cumbersome and fail in the crossover region of degenerate excitations. As noted in the Introduction, the alternation δ is related to the coherence length of infinite chains and to the convergence of oligomers to infinite chains. The choice $\delta=0.6$ corresponds to $t_- = t_+/4$, with substantial but smaller delocalization than realized in conjugated polymers.

The large but finite basis of (1) allows exact solutions, currently to $2N=14$ sites with a Silicon Graphics computer.³⁸ Energy thresholds for triplet, one-photon, and two-photon excitation of excitonic chains with $\delta=0.6$ and open boundary conditions are listed in Table I. We used the Ohno potential (16) for hydrocarbons and the PA geometry in Fig. 1. In order to place $2A$ slightly below $1B$, we took $t_+ = -2.0$ eV and $t_- = -0.5$ eV. We first note that all thresholds in Table I are close to convergence for seven dimers. Convergence is faster for larger δ , slower for smaller δ . We then compare with the first-order estimates (15) for H_0 at $\delta=1$, which are $\epsilon_t = 2.612$ and $E_b = 5.725$ eV for these parameters. As expected for CT stabilization (24) of $|TT1\rangle$, we have $E(2A) < 2\epsilon_t$. These $\delta=0.6$ oligomers hardly require extrapolation and are close to crystal results at $\delta=1$. Table II lists the same thresholds of Hubbard chains with $t_{+/-} = -2.0/-0.5$ eV and $U=5.0$ eV, again with $2A$ just below $1B$. The convergence is comparable and the estimates (15) and (19) now yield $\epsilon_t = 2.217$ eV and $E(1B) = 4.586$ eV at the CT band edge. The Hubbard chain also has $E(2A) < 2\epsilon_t$, as expected¹¹ on general grounds.

The convergence illustrated in Tables I and II is supported by all other calculations on shorter or cyclic oligomers on either side of the $1B/2A$ crossover. Similar convergence is found³⁹ in antiferromagnetic Heisenberg chains, the strong-coupling limit of (1), with alternating exchange constants $J(1 \pm \delta)$; the ground state and ϵ_t converge for $\delta=0.2$ in spin chains and rings up to $N=22$ and 28, respectively. For the band limit, with $U=0$, we use analytical results for cyclic oligomers with $Q=4n+2$ sites and nondegenerate ground states. The Hückel gap between filled and empty orbitals approaches the band limit $4t\delta$ as

$$\Delta E(Q)/4t\delta = [1 + (\delta^{-2} - 1)\sin^2\pi/Q]^{1/2} . \quad (26)$$

Thus $Q=14$ is $\sim 4\%$ from the converged value for

TABLE I. Energy thresholds, in eV, of $2N$ -site chains with $t_+ = -2.0$ eV and $\delta=0.60$ in Eq. (1), the Ohno potential $V(p,p')$ in Eq. (16), and PA geometry in Fig. 1; E_T is the lowest triplet, $E(2A)$ and $E(1B)$ the lowest even and odd singlets, and $-E_g/N$ is the ground-state energy per site.

$2N$	E_T	$E(2A)$	$E(1B)$	$-E_g/N$
8	2.5165	4.9187	5.4472	1.3213
10	2.5099	4.9097	5.3717	1.3224
12	2.5060	4.9054	5.3203	1.3231
14	2.5035	4.9031	5.2835	1.3237
polymer	2.50	4.90	5.20	1.335

TABLE II. Energy thresholds, in eV, of $2N$ -site Hubbard chains with $U=5.0$ eV, $t_+ = -2.0$ eV, and $\delta=0.60$; E_T is the lowest triplet, $E(2A)$ and $E(1B)$ the lowest even and odd singlets, and $-E_g/N$ is the ground-state energy per site.

$2N$	E_T	$E(2A)$	$E(1B)$	$-E_g/N$
8	2.1220	4.1677	4.8282	1.1248
10	2.1154	4.1549	4.7239	1.1259
12	2.1114	4.1482	4.6574	1.1266
14	2.1088	4.1445	4.6124	1.1272
polymer	2.10	4.13	4.50	1.13

noninteracting electrons at $\delta=0.6$. To first approximation, convergence depends on the alternation for any U and $V(p,p')$ in (1). The convergence of higher-energy excitations in Figs. 3 and 4 is less rapid, but adequate to $\sim 1.5E_b$. NLO coefficients of Hückel chains explicitly illustrate various size and alteration dependencies.⁴⁰

The first-order excitations (15) and (19) are for $k=0$ crystal states at $\delta=1$. We compare them below to $k=0$ excitations of cyclic oligomers with $\delta=0.6$. Our goals are, first, to see whether the pattern of $J=1$ and -1 states in Figs. 3 and 4 is preserved near the spin-charge crossover and, second, to analyze the exact excitations in terms of TT , CT , and other crystal states in the dimer limit. To illustrate excitation patterns, we consider the $k=0$ excitations for $2N=10$ and classify them according to dimer states. There is one crystal state (11) with an excited dimer, two states $|TT1\rangle$ and $|TT2\rangle$ in (13), and two pairs of CT states $|CT1, \pm 1\rangle$ and $|CT2, \pm 1\rangle$ in (14). There are two ways of exciting three triplets, each of which generates a $k=0$ singlet TTT state, two $k=0$ singlets based on $TTTT$, and various combinations of a triplet with CT excitations in either the $J=1$ or -1 manifolds. Larger rings with $2N=12$ or 14 have an additional TT or CT state. A known number of TT states is consequently predicted below E_b in excitonic systems.

The lowest-energy $J=1$ and -1 singlets of excitonic rings with $\delta=0.6$ are shown in Fig. 5 in the crossover region, in units of E_b in (15), for the Ohno potential (16) and PA geometry. The solid and dashed lines are $J=1$ and -1 excitations of H_0 taken from Fig. 3. Each intradimer mixing 2ϕ in Fig. 5 provides a direct comparison between exact oligomers with $\delta=0.6$ and infinite chains with $\delta=1$. The expected ordering of low-lying states is found on both sides of the crossover, as summarized in Appendix B for $2N=10, 12$, and 14 .

Excitations of Hubbard rings in the crossover region are shown in Fig. 6 in units of E_{CT} , again for $2N=10, 12$, and 14 . The solid and dashed lines for $J=1$ and -1 are taken from Fig. 4. Electron transfer between dimers again splits the TT states (13) on either side of the crossover. The crystal energy $E(1B)$ is the red edge of the CT band (19). The $|CT1, \pm 1\rangle$ and $|CT2, \pm 1\rangle$ states for $N=5$ lead to a 2×2 matrix in (18) whose bandwidth is half that of the infinite chain. Three CT states for $2N=14$ give a 3×3 matrix whose bandwidth is $\sim 70\%$ of the infinite chain's. As noted in Appendix B, four CT states appear for $N=5$, two with each J , while $N=7$ generates six CT states. The complicated excitation patterns

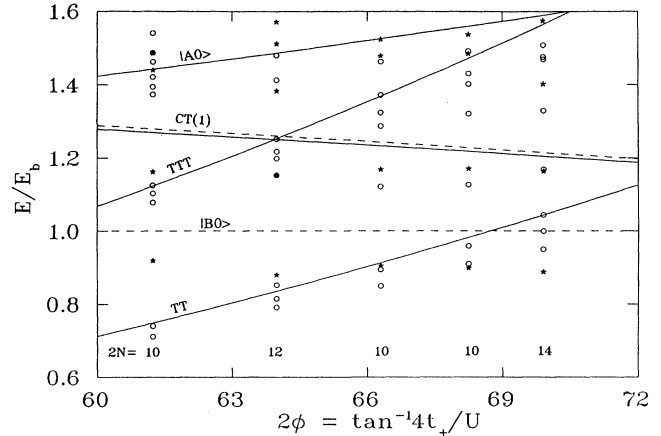


FIG. 5. Exact excitation energies of $2N$ -site cyclic oligomers with $\delta=0.6$ and the Ohno potential (16) for the PA geometry in Fig. 1, in units of E_b in Eq. (15) for the infinite chain of dimers. Open circles and closed stars are $k=0$ singlets with $J=1$ and -1 , respectively. The solid and dashed lines are crystal excitations from Fig. 3. The splitting of oligomer excitations by $H_-(\delta)$, Eq. (3), is discussed in the text.

in Fig. 6 are readily interpreted up to $\sim 1.5E_b$ in terms of crystal states with excited dimers. The $J=1$ dimer excitation E_a in (15) has high energy in Hubbard chains, above the states in Fig. 6.

Dimer excitations (15) and (19) clarify the nature of low-lying states in the crossover region of both excitonic and Hubbard chains with $\delta=0.6$. With $t_- \sim -0.5$ eV, however, we expect nearby excited states to mix and analyze the mixing by expanding the normalized oligomer eigenstates in the (complete) dimer basis. We again consider $k=0$ singlets with $J=1$ or -1 and write

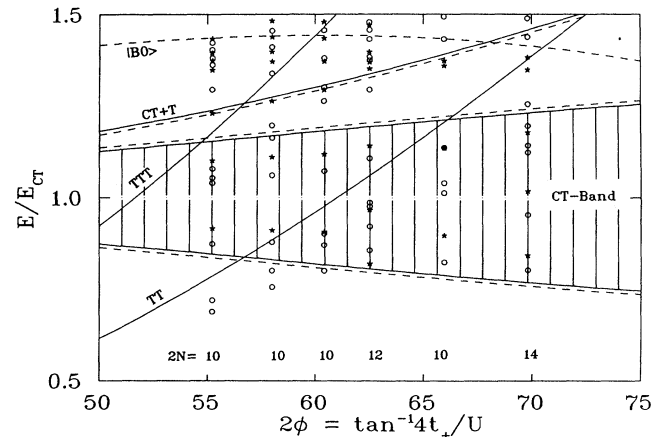


FIG. 6. Exact excitation energies of $2N$ -site cyclic oligomers with $\delta=0.6$ and Hubbard potential U , in units of E_{CT} in Eq. (15) for the infinite chain of dimers. Open circles and closed stars are $k=0$ singlets with $J=1$ and -1 , respectively. The solid and dashed lines are crystal excitations from Fig. 4; only the lower edge of the $CT+T$ band is shown. The splitting of oligomer excitations by $H_-(\delta)$, Eq. (3), is discussed in the text.

The linear spectrum is simple for excitonic chains when $|CT1, -1\rangle$ is a proper zeroth-order function. Its mixing with $|B0\rangle$ leads to

$$\begin{aligned} |1B\rangle &= \cos\beta|B0\rangle + \sin\beta|CT1, -1\rangle, \\ |2B\rangle &= -\sin\beta|B0\rangle + \cos\beta|CT1, -1\rangle, \end{aligned} \quad (28)$$

with

$$\tan 2\beta = t_-(\cos\varphi + \sin\varphi) / [E_{CT}(1) - E_b].$$

Transition dipoles with $|G\rangle$ involve only $|B0\rangle$ in lowest order and partition the intensity $N\mu_b^2$ in (20) as $\cos^2\beta$ for the exciton and $\sin^2\beta$ for the CT state. The mixing of $|B0\rangle$ and the CT band (19) in Hubbard chains is similar except that the coefficients c_{p1} in (23) are used for the eigenfunctions $|CTp, -1\rangle$. Transition moments $\langle m^1B_u|\mu|G\rangle$ with $m=1, 2, \dots$ appear in the linear spectrum of open chains. The two-photon transition moment M_a is given by (21) in the dimer limit. The most important intermediate state is $1B$ in conjugated polymers, $|B0\rangle$ in the dimer limit. The corresponding expression for chains is

$M(nA)$

$$= \sum_m \langle nA|\mu|mB\rangle \langle mB|\mu|G\rangle / [E(mB) - E(nA)/2] \quad (29)$$

for even-parity states $|n^1A_g\rangle$ with excitation energy $E(nA)$. We use the lowest 10–15 odd-parity states in the sum, an approximation that has previously been tested²⁶ against exact $M(nA)$ in PA chains with smaller δ , and exact transition dipoles and excitation energies. Two-photon intensity for TT states requires CT contributions (24) and transition dipoles (25) between CT states.

We present in Figs. 7 and 8 transition dipoles $\langle m^1B_u|\mu|G\rangle$ and $M(nA)$ for excitonic chains of $N=4$ and 5 dimers on either side of the spin-charge crossover, while Figs. 9 and 10 show the corresponding Hubbard moments. We took alternation $\delta=0.6$ throughout, again used the Ohno potential (16) for the PA geometry in Fig. 1, and chose identical intradimer correlations to the cyclic oligomers in Figs. 5 and 6. All transition dipoles are along the polymer backbone. These representative spectra are discussed separately.

The excitonic chain in Fig. 7 has $N=4$ and 5, $U_e/t_+ = 1.757$, $t_+ = -2.0$ eV, and $\delta=0.6$. Its excitation thresholds appear in Table I, while the $k=0$ states of cyclic oligomers are the $2\varphi=66.29^\circ$ column in Fig. 5 and the $k=0$ expansion in terms of dimer states is given in Tables III and IV for $N=5$. Different boundary conditions do not change the pattern of TT and CT states in the $J=1$ manifold [Fig. 7(a)] or of exciton and CT states with $J=-1$ [Fig. 7(b)]. Loss of translational symmetry simply increases the number of transitions in each energy regime, as indicated in Appendix B. We find the expected number of TT states, four for $N=4$ and six for $N=5$. We also expect four and six CT states with adjacent charges for $N=4$ and 5, respectively, and they are easily counted in Fig. 7. The $J=-1$ exciton gives two and

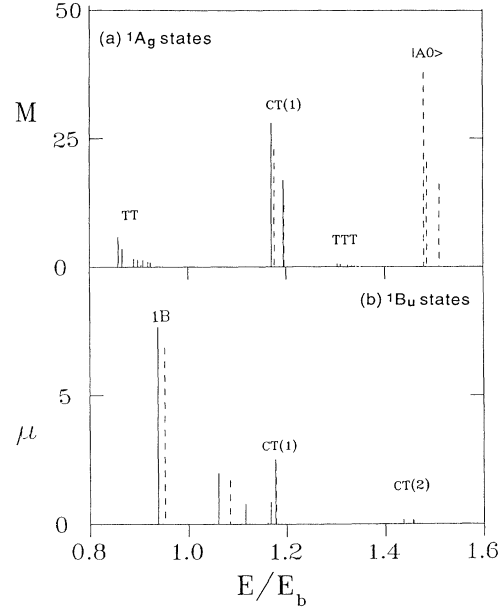


FIG. 7. Transition moments μ (b) in D, and M (a) in D^2/eV for linear and two-photon absorption of $2N$ -site excitonic chains, on the correlated side of the spin-charge crossover, with $\delta=0.6$ and the Ohno potential (16) for the PA geometry in Fig. 2. Solid and dashed lines are for $N=5$ and 4, and energies are in units of E_b , Eq. (15). Spectra in (a) extend to $1.5E_b$ for $N=4$ and to $1.4E_b$ for $N=5$, as discussed in the text.

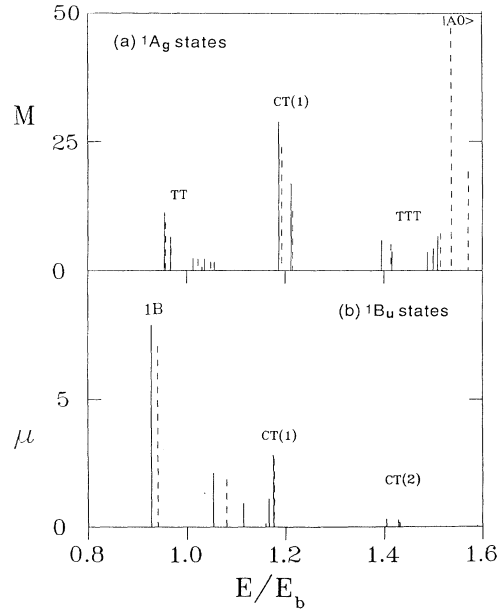


FIG. 8. Same as Fig. 7, but with $2A$ above $1B$, on the band side of the spin-charge crossover. Spectra in (a) extend to $1.5E_b$ for $N=5$.

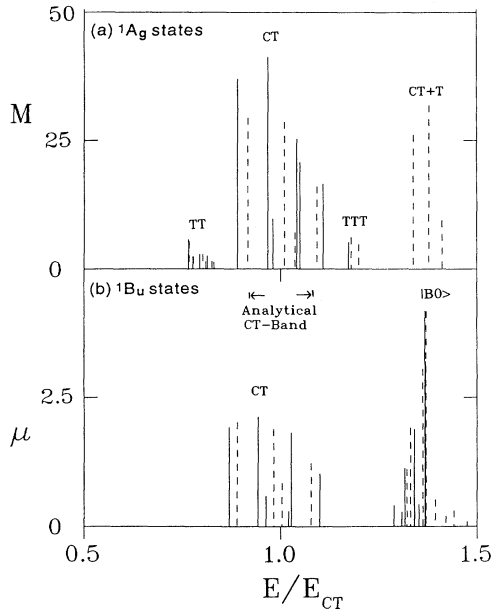


FIG. 9. Transition moments μ (b) in D and M (a) in D^2/eV for linear and two-photon absorption of $2N$ -site Hubbard chains with $\delta=0.6$, on the correlated side of the spin-charge crossover. Solid and dashed lines are for $N=5$ and 4, and energies are in units of E_{CT} , Eq. (15). Spectra in (b) extend to $1.38E_{CT}$ for $N=5$ and in (a) to $1.4E_{CT}$ and $1.17E_{CT}$ for $N=4$ and 5, respectively.

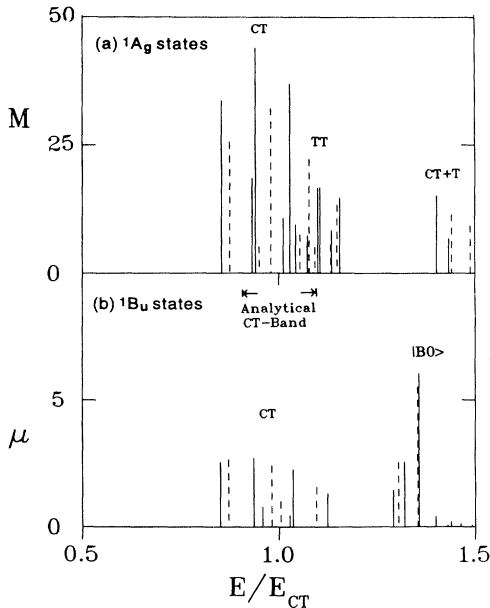


FIG. 10. Same as Fig. 9, on the band side of the spin-charge crossover. Spectra in (a) extend to $1.43E_{CT}$ for $N=5$.

three lines for $N=4$ and 5, with greatest intensity at lowest energy. Transition dipoles for $|CT1, -1\rangle$ states in Fig. 7(b) are realizable in the first-order mixing (28). The smaller moments for $|CT2, -1\rangle$ reflect a higher-order process in t_- , with minimally two interdimer electron transfers. The mixing of these CT states, given in Table IV for $N=5$ rings, supports the analysis in terms of dimer states.

The two-photon transition moments in Fig. 7(a) are quite different from the dimer limit. The E_a excitation around $1.5E_b$ gives the two lines expected for $N=4$. Spectral congestion and the limitation to ~ 15 exact excitations restrict the two-photon spectrum to $1.5E_b$ for $N=4$ and to $1.4E_b$ for $N=5$, so that E_a does not appear. Interdimer electron transfer is needed for all A_g states (29) related to TT , CT , TTT , and $CT+T$ excitations. Beyond the dimer limit, the matrix elements $\langle m^1B_u | \mu | G \rangle$ in (29) do not vanish for composite excitations in (22), (24), or (28). The transition moments (25) connecting CT states then imply appreciable two-photon intensity $M(nA)$ for $|CT1, 1\rangle$ even in first order, as corroborated in Fig. 7(a). The appearance of intense $CT+T$ states at higher energy in Fig. 7(a) is beyond low-order perturbation theory, but can be rationalized in terms of strong mixing of $|CT2, 1\rangle$ and nearby $J=1$ states.

Only intradimer correlations $U_c/t_+ = 1.464$ for $t_+ = -2.4$ eV have been changed for the excitonic chain in Fig. 8 on the band side of the crossover. The corresponding $k=0$ excitations of rings are the $2\varphi=69.9^\circ$ column in Fig. 5, whose general pattern is retained in chains. We now have larger $t_- = -0.6$ eV at $\delta=0.6$. The linear moments in Fig. 8(b) hardly change when S_1 becomes $1B$; slightly greater CT contributions are consistent with larger t_- and smaller $E_{CT1} - E_b$. Two-photon moments in Figs. 8(a) and 7(a) are also qualitatively similar. Distinctly larger $M(nA)$ in the TTT region of Fig. 8(a) are rationalized by their proximity to CT states and are again beyond low-order perturbation theory. The dimer state E_a appears for $N=4$ and the $N=5$ spectrum in Fig. 8(a) extends to $1.5E_b$.

Near the dimer limit, two-photon intensities of TT states are entirely due to admixtures of CT states in either Hubbard or excitonic systems and go as t_-^4 to lowest order according to (29) or (21). Since CT states appear in first order, $M(CT)^2$ goes as t_-^2 . Two-photon transition moments for the lowest TT and CT states are given in Table V for $N=4$ using the energies in Table I for excitonic chains and in Table II for Hubbard chains. They confirm the perturbation analysis, which indeed holds in general for excitonic chains when t_- is sufficiently small compared to energy denominators $E_{CT} - 2\epsilon_t$ and $E_{CT} - E_b$ in the $J=1$ and -1 manifolds. Table V indicates deviations at $t_- = t_+/4$ from lowest-order perturbation theory. Since $E_{CT} - 2\epsilon_t$ and $E_{CT} - E_b$ are equal at the $2A/1B$ crossover, stronger TT intensity above the $2A/1B$ crossover in Fig. 8(a) reflects smaller, but still finite, denominators in excitonic systems and slightly larger t_- at constant δ .

The transition dipoles in Figs. 9 and 10 are for Hubbard chains with $N=4$ and 5 on either side of the $2A/1B$

crossover. The $U/t_+ = 2.5$, $t_+ = -2.0$, $\delta = 0.6$ results in Fig. 9 go with the energy thresholds in Table II and the $k=0$ excitations for $2\varphi = 57.99^\circ$ in Fig. 6. The linear spectrum for $N=5$ extends to $1.38E_{CT}$, the two-photon spectrum to $1.17E_{CT}$ for $N=5$ and to $1.4E_{CT}$ for $N=4$, where E_{CT} is the analytical result (15). The linear spectrum in Fig. 9(b) has E_b above the CT band of four and six states for $N=4$ and 5, respectively. The CT transition moments are large and the symmetric distribution (23) of c_{p1} expected about E_{CT} in first order is distorted to the low-energy side in Fig. 9(b). With low-energy CT states, we also have $CT+T$ singlets appearing in the linear spectrum and their intensities are beyond low-order perturbation theory. The two-photon transition moments of Hubbard chains with $S_1 = 2A$ in Fig. 9(a) resemble the excitonic results in Fig. 7(a), in accord with Table V. The number of low-energy TT states is the same, while greater intensity reflects the proximity of the CT band, in which $|CT1, 1\rangle$ is distributed according to (23). There are many CT states in the Hubbard band, as well as TTT and $CT+T$ states in the $J=1$ manifold whose mixing in the TTT region of Fig. 9(a) first appear as t_-^4 . The dimer state at E_a is considerably higher.

The transition moments in Fig. 10 are for Hubbard chains on the opposite side of the crossover, with $t_+ = -2.8$ eV and the same U and δ as in Fig. 9. The $k=0$ singlets for $2\varphi = 65.94^\circ$ in Fig. 6 are the corresponding excitations. The linear spectrum in Fig. 10(b) does not change significantly. We have the expected number of CT states, higher intensity for larger $t_- = -0.7$ eV at $\delta = 0.6$, and singlet excitons derived from $|B0\rangle$; the $CT+T$ excitations shift to higher energy and become more intense. The two-photon moments in Fig. 10(a) are fundamentally different, however, now that the lowest $J=1$ singlet is a CT state. Thus $M(nA)$ for $n=2, 3, \dots$ is much larger in Fig. 10(a) than in Fig. 9(a), where these were TT states. We count CT states for $N=4$ and 5 to identify the TT states in Fig. 10(a), but these nearly degenerate states are strongly mixed. The singlet A_g spectrum is less congested because TTT states shift to higher energy with decreasing correlations.

The $2A/1B$ crossover in Hubbard models is fundamentally different because the energy denominator $E_{CT} - 2\epsilon_t$ vanishes. Finite t_- in (24) then strongly mixes TT and CT states at the crossover and low-order perturbation theory fails. CT states dominate the two-photon threshold in Fig. 10(a) on the band side, and their number grows with N . We therefore expect TT contributions in infinite Hubbard chains to be negligible when $2A$ be-

comes a CT state, except possibly right at the crossover. We emphasize that different spin-charge separation in Hubbard and excitonic systems is due to different $J = -1$ excitations in Figs. 3 and 4 rather than the actual energies. Since all symmetries are the same for any $\delta > 0$ in (1), different crossovers are expected in general.

Transition moments similar to Figs. 7–10 can readily be generated and analyzed for any quantum cell model (1) up to $2N = 14$. This suffices for any NLO coefficient in the dipole approximation. Both linear and cyclic oligomers follow, at least for $\delta \geq 0.6$, crystal states constructed at $\delta = 1$ for an infinite chain. The low-energy excitations in Figs. 7–10 cover a tiny fraction of the spectrum. We estimate the contribution of other excitations through a sum rule, without finding individual transition dipoles. The identity³⁵

$$\sum_P |\langle P|\mu|X\rangle|^2 = e^2 W(X)N = e^2 \sum_{pp'} \mathbf{r}_p \cdot \mathbf{r}_{p'} \langle X|q_p q_{p'}|X\rangle \quad (30)$$

holds for any correlated state $|X\rangle$ of quantum cell model (1) and relates transition dipoles to the mean square separation $W(X)$ of charge fluctuations in $|X\rangle$. We evaluate $W(G)$ and compare to the sum over squares of individual transition moments in Figs. 7(b)–10(b). The linear spectra shown account for more than 99% of $W(G)$ for either $N=4$ or 5.

Contributions of high-energy states to two-photon spectra are more difficult to assess and are not limited by sum rules. In excitonic chains, when $|^1B_u\rangle$ dominates in (29), we can evaluate $W(1B)$ and compare with the transition moments $\langle nA|\mu|1B\rangle$ found directly. Analysis of PPP chains²⁶ with small δ showed important contributions from a two-photon state around E_a that we related to two-electron excitation. At large δ , however, the linear spectra in Figs. 7(b)–10(b) have many additional lines, especially in Hubbard models. Since the transition moment (29) diverges at $E(mB) = E(nA)/2$, large contributions can appear for weakly coupled states, as illustrated by $CT+T$ features in Figs. 8(a) and 10(a). The transition dipole (21) gives the entire two-photon intensity at $t_- = 0$ and M_a is $\sim 25 D^2/\text{eV}$ in the crossover region, comparable to the $M(nA)$ in Figs. 7(a)–10(a) associated with CT states and larger than TT moments. We conclude that two-photon intensities increase more rapidly than the linear spectrum with increasing delocalization.

V. DISCUSSION

We have obtained low-lying correlated states of quantum cell models (1) with intermediate correlations, arbitrary spin-independent potential $V(p, p')$, and large alternation $t_\pm = t(1 \pm \delta)$ along the PA backbone in Fig. 1. The molecular-exciton states in Sec. II and Appendix A are general many-electron functions near the dimer ($\delta = 1$) limit. The physical interpretation of crystal states with one or several excited dimers clarifies the analytical excitations (15) and (19) at the spin-charge crossover for any $V(p, p')$ and $\delta \geq 0.6$. In contrast to well-separated excitations in organic molecular crystals, degeneracies

TABLE V. Two-photon transition moments $M(TT)$ and $M(CT)$, in D^2/eV , of the lowest TT and CT states of $N=4$ excitonic chains in Table I and, in parentheses, $N=4$ Hubbard chains in Table II.

$-t_-$ (eV)	$M(TT)/t_-^2$	$M(CT)/t_-$
0.01	31.5 (31.1)	43.6 (53.0)
0.10	33.2 (26.2)	44.3 (52.8)
0.30	28.0 (22.7)	46.8 (57.6)
0.50	19.4 (21.0)	45.5 (58.2)

are intrinsic at the crossover and crystal states are strongly mixed by interdimer electron transfer t_- . We then exploit short coherence lengths at large δ to obtain linear and two-photon spectra in terms of oligomers containing up to $N=7$ dimers. Tables I and II show the convergence with N of threshold energies of excitonic and Hubbard chains. These correlated crystal states make possible a detailed analysis of spin-charge crossovers at intermediate correlations $U \sim 2t_+$, small t_- , and arbitrary $V(p,p')$ in (1), where neither band nor strong-coupling methods are applicable.

Although motivated by NLO spectra and correlated states of conjugated polymers,⁴⁵ our results are not directly applicable to these more delocalized, less alternating, systems with 10 eV bandwidths. Typical values²⁶ are $\delta = \frac{1}{3}$ in polysilanes (PS's), $\delta = 0.15$ in polydiacetylenes (PDA's), $\delta = 0.07$ in PPP models of polyenes or PA, and effective δ_e between the PS and PDA values for poly-*p*-phenylenevinylenes⁴⁶ (PPV's) and polythiophenes (PT's).⁴⁷ PPP models with molecular parameters account¹⁰ for strong fluorescence in PS's or PPV's and weak or extrinsic emission in PDA's or PA. The present analysis provides reliable excitations in the crossover region for large δ and bears directly on the location and intensities of even-parity states of quantum cell models (1) proposed for conjugated polymers.

We deliberately chose the Ohno potential (16) for excitonic chains. The PPP model^{48,7} gives the best fits for π - π^* spectra of conjugated molecules within a π -electron approximation. Its parameters⁴⁹ and the Ohno potential³⁶ have been extensively applied to conjugated hydrocarbons. No adjustable parameters are needed for linear and two-photon excitations of polyenes,⁷ anthracene,⁵⁰ or other conjugated molecules, and a similar potential holds²⁵ for σ -conjugated silanes. In effect, we have in $V(p,p')$ a good approximation for semiconducting polymers, where shielding of Coulomb interactions is not an issue. Small (10%) refinements of parameters for the solid state are secondary here compared to the identification of the conjugated-polymer sector of the quantum cell models (1).

The $2A/1B$ crossover of PPP models with the Ohno potential and a realistic bandwidth of $4t = 9.6$ eV is near⁵¹ $\delta = 0.20$. While oligomer excitations have not converged at $2N = 14$ for small δ , sensible $E(2A)/E(1B)$ extrapolations are possible for conjugated polymers and $E(1B)$ provides²⁶ a convenient internal standard for NLO spectra. Recent two-photon spectra for PA films,⁵² for PDA-PTS single crystals,⁵³ and for PPV films⁵⁴ are consistent with prior PPP assignments.²⁶ Such data illustrate that increasing δ at constant bandwidth and $V(p,p')$ effectively decreases e - e correlations.^{10,45} At larger $\delta = 0.60$ and the same potential, the bandwidth must be reduced to 5.0 eV in Table I to place $2A$ below $1B$. The $1B/2A$ crossover in Hubbard models with increasing δ also occurs a smaller bandwidth, around $U = 4t$ for $\delta = 0.6$ in Table II rather than $U \sim 2t$ for $\delta \sim 0.1$. Faster convergence of oligomers at larger δ also implies weaker correlations that must explicitly be compensated to preserve the $2A$ - $1B$ order.

The theoretical challenge is to follow the evolution of

oligomers into bands for arbitrary parameters in (1), not just in the noninteracting limit. In Hückel chains, $2A$ is the band edge and linear, two-photon, or third-harmonic generation, spectra are readily found^{55,40} up to $2N \sim 400$. They evolve to the band results of Agrawal, Cojan, and Flytzanis,³⁰ who demonstrated a two-photon peak a few percent above $E(1B) = 4t\delta$ with rigorously vanishing $M(2A)$. Oligomer calculations also show $M(2A)$ to vanish at large N and are understood^{31,26} in Hückel chains as destructive interference due to e - h symmetry. In units of the band gap $4t\delta$, the two-photon peak²⁶ associated with one-electron excitations hardly depends on δ .

The magnitude of $M(2A)$ has been less clear in interacting chains. In the essential-states model,⁵⁶⁻⁵⁹ negligible M 's are predicted for $2A$ and other even-parity states below $E(1B)$ for all parameters in the quantum cell models (1), and tiny $M(2A)$ has also been proposed⁵⁹ when $E(2A)$ is above $E(1B)$ in PS or PPV. Essential states are identified through their transition dipoles, primarily with $1B$, in exact solutions of extended Hubbard chains of $N = 2-5$ dimers. The largest transition moment with $1B$ identifies the mA_g state that is found between $E(1B)$ and $E(2B)$ for chains with quite different t_+ , t_- , U , V_1 , V_2 , or $V(p,p')$ in (1). Such behavior inferred from hundreds of specific calculations is taken to be universal.⁵⁸ Artificially large alternation is used to facilitate convergence, but the location of excited states is taken from experiment⁵⁷ and from internal constraints such as the location of mA_g . A major conclusion^{58,59} is the occurrence of similar THG and NLO spectra for half-filled chains (1). This extends the band results, which gave similar spectra in units of the gap $4t\delta$, to interacting systems and is also consistent⁶⁰ with strong correlations $U \gg t$, where spin waves do not contribute and NLO responses start at $E(1B) \sim U$. Hubbard spectra in Figs. 9 and 10 show an onset of two-photon intensity around E_{CT} at the spin-charge crossover, when TT and CT states cross in the $J = 1$ manifold. Strong two-photon absorption at the crossover is consistent with the essential-states model, with mA_g a CT state in Hubbard models, but differences emerge below for excitonic chains.

The present analysis also relies on oligomers, but is complemented by analytical results for crystal states. Detailed information about converged crystal states in the crossover region clarifies the magnitude of $M(2A)$ and differentiates between the $2A/1B$ crossovers of excitonic and Hubbard chains. In half-filled Hubbard chains, we rigorously have $M(2A) = 0$ in the band ($U = 0$) limit³⁰ for any δ and in the dimer ($t_- = 0$) limit for any U . Since the dimer excitations (8) are finite, perturbation theory holds at sufficiently small t_- and gives the first-order splittings (19) about E_{CT} in (15). The c_{p1} coefficients (23) then show $M(2A)$ to vanish in infinite Hubbard chains with $\delta \sim 1$ as long as $2A$ is a CT state; the band result is retained for $U < 2t_+$. For $U > 2t_+$, on the other hand, $2A$ becomes a TT state and the magnitude of $M(2A)$, which goes as t_-^2 according to (29) or Table V, depends on the admixture of CT states and the energy denominators $E_{CT} - E_{TT}$ and $E_{CT} - E_b$ in the $J = 1$ and -1 mani-

folds. The latter imply vanishing $M(2A)$ in the spin-wave limit ($U \gg t_+$), while $t_- = 0$ ensures vanishing TT intensity in the dimer limit for any N . The TT band thus acquires two-photon intensity on the correlated side of Hubbard chains [Fig. 9(a)]. To lowest order in t_- , the TT bandwidth goes as $t_-^2 / (E_{CT} - E_{TT})$ and $2A$ defines its red edge. We have not found $M(2A)$ explicitly, but the stabilization (24) of $|TT1\rangle$ by CT states supports finite $M(2A)$ for the band-edge state.

The behavior of excitonic chains depends on the relative magnitudes of U , V_1 , and $V(p, p')$. We still have $M(2A) = 0$ in the band limit at the red edge $4t\delta$ of one-electron excitations, while $t_- \sim 0$ places the lowest TT state at $8t\delta$, twice as high. Increasing $V(p, p')$ in weakly correlated dimers whose TT states are well above the band edge generates an S_1 crossover between a CT state and a singlet exciton. This involves exciton formation rather than spin-charge separation, however, and different issues arise. Any chain whose lowest $J = -1$ singlet is $|B0\rangle$ is defined as “excitonic” in Fig. 3. The $2A/1B$ crossover in Figs. 7 and 8 then involves discrete levels and $M(TT)$ increases smoothly through the crossover, with finite energy denominators $E_{CT}(1) - E_{TT}$ and $E_{CT}(1) - E_b$ in (29). Stronger mixing eventually occurs on the band side of the crossover, when $E_{CT1} - E_{TT}$ vanishes in Fig. 3. The mixing (24) of $|TT1\rangle$ and $|CT1, 1\rangle$ again indicates finite $M(2A)$ at the edge of the TT manifold in the crossover region. These denominators become large for strong correlation and suppress²⁶ spin-wave contributions. As noted in connection with Figs. 7 and 8(a), $M(TT)$ at the crossover is about half as large as the dimer transition M_a in (21).

In contrast to the essential-states analysis,^{56–59} we find different NLO responses for Hubbard and excitonic chains with intermediate correlations, and excitonic chains provide examples in which mA_g is not between $E(1B)$ and $E(2B)$. Large δ and V_1 imply a narrow band of $|Bk\rangle$ states (11) above any TT state and below any CT with $J = 1$ in Fig. 3, without any even-parity states between $E(1B)$ and the entire band (12) about E_b . Oligomers in Fig. 7 illustrate spectra without A_g states between $1B$ and $2B$. Moreover, the state mA_g with the largest transition dipole to $1B$ is even higher, above $4B$ and $5B$ for $N = 5$ in Figs. 7 and 8, respectively. The problem is the enormous parameter space of alternating chains (1). The trapping^{56–59} of mA_g between $E(1B)$ and $E(2B)$ is a special case for some extended Hubbard models rather than⁵⁸ “universal.” An important advantage of our molecular-exciton approach is the straightforward searching of parameter space guided by analytical crystal states. As previously noted,²⁶ the localized representation of essential states is best at strong correlations where $|G\rangle$ becomes covalent in half-filled systems. The difficulty of essential states in the band limit is that, for alternating even and odd orbitals, $2A$ is the only even-parity state between $1B$ and $2B$, and vanishing $M(2A)$ is inconsistent for an essential state. The model for interacting chains is not analytical in the interaction.

Two-photon spectra of polyenes⁶¹ and THG spectra of β -carotene⁶² involve $2A$ and are consistent with finite

$M(2A)$ in the PPP model with $\delta = 0.07$. We also expect finite $M(2A)$ in conjugated polymers near the $2A/1B$ crossover. PA or PDA spectra then resemble Fig. 7, with $2A$ below $1B$, while PPV or PS excitations resemble Fig. 8, with $2A$ above $1B$. The TT and CT designations are only qualitative at small alternation, however, where $H_d(\delta)$ strongly mixes dimer excitations. PPP spectra for oligomers are then much sparser²⁶ than in Figs. 7 and 8. The two-photon excitation E_a is a biexciton that appears naturally in PPP models and, as indicated by the dimer excitations (8), shifts to higher energy on the band side. The strongest two-photon peak⁵³ of crystalline PDA-PTS is around $1.35E(1B)$, above the photoconductivity band edge⁶³ of $1.25E(1B)$. Larger $\delta = \frac{1}{3}$ for PS oligomers gave transition moments similar to Fig. 8, with $2A$ above²⁶ $1B$ and more intense as expected due to stronger mixing of CT states. Atomic data for Si in (16) place the biexciton E_a around³⁷ $1.8E(1B)$, consistent with two-photon, electroabsorption, and photoabsorption⁶⁴ spectra. The two-photon spectra in Figs. 7(a) and 8(a) indicate considerable mixing of $J = 1$ states around E_a , and such mixing at smaller δ further blurs CT and TT designations. It is, nevertheless, useful to follow the evolution of states and energy thresholds with increasing correlations. The E_a feature in Fig. 3 evolves from $2E(1B) = 8t\delta$ in the band limit to $\sim E(1B)$ in the limit $U_e \gg t$. The present results at large δ support the previous analysis²⁶ of PPP chains and provide considerably more information about the correlated states.

On the band side, when $2A$ is above $1B$, the spectra of excitonic chains in Fig. 8 can also be found in band theory^{15–17} with first-order CI and very good fits have been achieved⁶⁵ for linear, two-photon, and THG spectra of poly(di- n -hexylsilane) using a long-range potential similar to (16) with adjustable on-site repulsions and transfer integrals chosen specifically for the polymer. These excitonic models also yield finite $M(2A)$. First-order CI can be carried out for much longer chains of ~ 50 unit cells, which suffices for the relevant δ . On the other hand, the method is limited to the band side of the crossover, since additional CI is needed to have $2A$ below $1B$. The basis of $k = 0$ states with two e - h pairs increases rapidly as N^3 and size consistency becomes a major challenge for any truncation of the states. Exact analysis of oligomers with large δ covers both regimes without extrapolation, although direct solutions are not likely for ten dimers and even longer chains will be needed for convergence at small δ .

In summary, we have presented a molecular-exciton approach for finding excited states of half-filled quantum cell models (1) with arbitrary spin-independent $V(p, p')$, intradimer correlations U/t_+ , and large alternation δ . Exact analysis of linear and cyclic oligomers indicates converged energy thresholds at $\delta = 0.6$ with $N = 4$ – 7 dimers and supports the occurrence of crystal states based on excited dimers. Analytical results for crystal states account for low-energy $k = 0$ singlets with $J = 1$ and -1 needed for linear, two-photon, THG, or other NLO responses at intermediate correlations. Their mixing by interdimer transfer t_- is understood qualitatively, but

oligomer spectra also show higher-order corrections in t_- . In Hubbard chains, $1B$ is a CT state and the spin-charge crossover of TT and CT states leads to a sharp increase of two-photon absorption on the band side. In chains whose $1B$ is an exciton, by contrast, the two-photon intensity of TT states increases smoothly through the crossover and the dimer excitation E_a appears around $1.5E(1B)$ for the Ohno potential (16), consistent with previous PPP results at alternations realized in conjugation polymers. The spin, $e-h$, and translational symmetries of (1) lead quite generally to an S_1 spin wave with $J=1$ at strong correlations and a $J=-1$ band-edge state for weak correlations. Different spin-charge crossovers for excitonic and Hubbard chains are consequently expected at any alternation.

ACKNOWLEDGMENTS

We gratefully acknowledge the National Science Foundation for support of this work through Grant No. DMR-9300163 and Z.G.S. thanks D. S. Galvão, S. Ramasesha, S. Etemad, R. G. Kepler, and F. C. Spano for many stimulating discussions.

APPENDIX A: DIMER BASIS

The dimer ground state $|g\rangle$ in Fig. 2 is given in terms of the fermion operators $a_{p\sigma}^\dagger, a_{p\sigma}$ as

$$|g\rangle = [\cos\varphi(a_{2p-1,\alpha}^\dagger a_{2p,\beta}^\dagger - a_{2p-1,\beta}^\dagger a_{2p,\alpha}^\dagger)/\sqrt{2} + \sin\varphi(a_{2p-1,\alpha}^\dagger a_{2p-1,\beta}^\dagger + a_{2p,\alpha}^\dagger a_{2p,\beta}^\dagger)/\sqrt{2}]|0\rangle, \quad (\text{A1})$$

where $|0\rangle$ is the dimer vacuum. The crystal ground state $|G\rangle = |gg \cdots g\rangle$ has an N -fold product of fermion operators acting on the crystal vacuum. The even-parity state $|a\rangle$ in Fig. 2 has coefficients of $-\sin\varphi$ for the covalent (Heitler-London) singlet and $\cos\varphi$ for the ionic singlet. The odd-parity state $|b\rangle$ is

$$|b\rangle = [(a_{2p-1,\alpha}^\dagger a_{2p-1,\beta}^\dagger - a_{2p,\alpha}^\dagger a_{2p,\beta}^\dagger)/\sqrt{2}]|0\rangle. \quad (\text{A2})$$

The crystal state $|B_p\rangle$ with an excited dimer p contains (A2) and a product of $N-1$ factors from (A1). The singlet linear combination of triplets at dimer n and $n'=n+r$ is

$$|TTn,r\rangle = [(a_{2n,\alpha}^\dagger a_{2n'-1,\beta}^\dagger - a_{2n,\beta}^\dagger a_{2n'-1,\alpha}^\dagger) \times (a_{2n-1,\alpha}^\dagger a_{2n',\beta}^\dagger - a_{2n-1,\beta}^\dagger a_{2n',\alpha}^\dagger)/2]|0\rangle \times \prod_{p \neq n, n'} |g_p\rangle, \quad (\text{A3})$$

and corresponds to covalent singlets between sites on opposite sublattices. Since all these dimer states contain an even number of fermions, the phases of the crystal states (11) or (13) do not depend on the position of the excitations. Crystal states containing excited dimers are both conceptually and computationally convenient. The combination of neutral excitations is straightforward and leads to higher-energy excitations. We have one $S=0$ combination for three triplets n, n' , and n'' , while four

triplets lead to two singlets. The construction of $k=0$ linear combinations then involves two and three relative separations, respectively.

The ground state of $|D^+\sigma\rangle$ is

$$|D^+\sigma\rangle = [(a_{2p-1,\sigma}^\dagger + a_{2p,\sigma}^\dagger)/\sqrt{2}]|0\rangle, \quad (\text{A4})$$

and the electron is in the bonding orbital. The ground state of $|D^-\sigma\rangle$ is

$$|D^-\sigma\rangle = [(a_{2p-1,\sigma}^\dagger a_{2p,\alpha}^\dagger a_{2p,\beta}^\dagger - a_{2p,\sigma}^\dagger a_{2p-1,\alpha}^\dagger a_{2p-1,\beta}^\dagger)/\sqrt{2}]|0\rangle, \quad (\text{A5})$$

with the electron now in the antibonding orbital. Since the bracketed operators in (A4) and (A5) create charged dimers in the ground state, the singlet linear combination for a cation at n and anion at $n+r$ is

$$|D_n^+ D_{n+r}^-\rangle = 2^{-1/2} (|D_n^+\alpha\rangle |D_{n+r}^-\beta\rangle - |D_n^+\beta\rangle |D_{n+r}^-\alpha\rangle) \times \prod_{p \neq n, n+r} |g_p\rangle. \quad (\text{A6})$$

The crystal states (9) with electron-hole symmetry J are linear combinations of (A6) and the function with D^- at n, D^+ at $n+r$. There are four fermions per CT pair and phases are easily fixed.

We may also construct CT states in which one or both of the radical ions are in the excited state, with one electron in the antibonding orbital for D^+ and two for D^- . Such excitations are at least $2t_+$ higher in energy, however, and require additional notation. The even linear combination in (A6) is a triplet CT state with $S_z=0$, while a triplet dimer with $S_z=0$ is obtained from the covalent part of (A1) by changing the phase of the cosine term. The two triplets are combined to form singlet $CT+T$ excitations in Figs. 7–10. Composite states involving TTT singlets with $k=0$ symmetry are also constructed by considering products of dimer functions.

APPENDIX B: DIMER ANALYSIS OF EXACT OLIGOMER STATES

The $k=0$ singlets of excitonic chains are shown in Fig. 5 for cyclic oligomers. The column at $2\varphi=66.29^\circ$ (intrasite correlation $U_e/t_+=1.757$) corresponds to $2N=10$, has $t_-=-0.5$ eV at $\delta=0.6$, and is on the correlated side of the crossover. We expect and find two TT states with $k=0$ and $J=1$ for $N=5$. Here S_1 is $2A$, with large contribution from $|TT1\rangle$ and small admixture of $|CT1,1\rangle$ as indicated in (24). The next $J=1$ state is $|TT2\rangle$. The lowest $J=-1$ singlet, $1B$, is $|B0\rangle$ by definition in excitonic chains and contains a small admixture of $|CT1,-1\rangle$ according to (22). At higher energy, we encounter a $J=1$ and -1 singlet whose major weight in Tables III and IV comes from $|CT1,1\rangle$ and $|CT1,-1\rangle$, respectively. At higher energy we expect and find two TTT states followed by two other $J=1$ states. Overlap analysis in Table III shows the first one to have a large $CT1+T$ component as well as appreciable $CT1$ and TTT contributions. The second $J=1$ state is clearly the dimer state $|A0\rangle$, which is seen in Table III

to be negligibly mixed for these parameters. Higher $J = \pm 1$ states have contributions from $CT2$ and other CT states that preclude a simple assignment.

Still in Fig. 5, we consider the $2N=14$ column at $2\varphi=69.9^\circ$, whose reduced correlations $U_e/t_+=1.464$ place it on the other side of the crossover; t_- has increased to -0.6 eV at $\delta=0.6$. S_1 is now largely the $|B0\rangle$ exciton. The next three $J=1$ singlets are TT states with $r=1, 2,$ and 3 possible for $N=7$; the lowest one is $|TT1\rangle$. The $|CT1,1\rangle$ and $|CT1,-1\rangle$ states are above the TT states. Both the increased t_- and smaller splitting between TT and CT states at $2\varphi=69.9^\circ$ increase the mixing of these states. As we go higher in energy, we encounter four TTT states with $J=1$ for $N=14$, the dimer state E_a , and both $CT2$, $CT+T$ states. The latter also appear in the $J=-1$ manifold.

The Hubbard excitations in Fig. 6 feature the CT bands (19) with $J=1$ and -1 . At $2\varphi=57.99^\circ$ ($U/t_+=2.5$), the two TT states for $2N=10$ are the lowest singlets at $t_-=-0.5$ eV ($\delta=0.6$). Their greater stabilization compared to excitonic chains is understood in terms of the smaller gap between TT and CT states. The lowest $J=-1$ singlet is a CT state. For $N=5$, the t_- matrix elements (18) lead to four CT states with the same parity as the first four states of a particle in a box. The $J=1$ (A_g) and -1 (B_u) states indeed alternate in the band and the width is smaller than in the crystal limit (18), although neither the energies nor the reduction of the bandwidth agree quantitatively with (19). The exact $J=1$ CT states are mixed with the TT states, while the $J=-1$ CT states mix with $|B0\rangle$ at E_b . We again have two TTT states with $J=1$ for $N=5$ and $CT+T$ states at the highest energy; the analytical first-order $CT+T$ lines for $J=1$ and -1 pass through the upper right corner of Fig. 6 and form the red edge of another band. The E_a state is still higher in Hubbard models, as expected from the dimer relation (8).

The excitations at $2\varphi=69.8^\circ$ ($U/t=1.471$) in Fig. 6 are on the opposite side of the crossover and have larger $t_-=-0.85$ eV ($\delta=0.6$). Since S_1 is now associated with the edge of the CT band, we expect degenerate $J=1$ and -1 singlets in infinite chains. The CT band (19) for $2N=14$ contains six states, three each with $J=1$ and

-1 , whose nodal properties are those of the first six states of a particle in a box. We also expect and find three $J=1$ states corresponding to TT states in the CT band, while the $J=-1$ state associated with $|B0\rangle$ is slightly above. There is less congestion in Hubbard models with $2\varphi=69.8^\circ$ and $\delta=0.6$. One reason is that TTT and $CT+T$ states are higher on the band side; another is that all CT states are now in the band, rather than spread out as shown in Fig. 3 for an excitonic chain.

Similar analyses can be carried out for other exact oligomer eigenstates. They are reasonable approximations for correlated crystal states at alternation $\delta=0.6$ or higher, not only for threshold energies, but up to $\sim 1.5E(1B)$ in the crossover regime. The strengths of an excitonic approach to crystal states are the correct ordering of states in the crossover region and their straightforward interpretation in terms of dimer excitations, which more than compensate the qualitative fits for the analytical excitation energies (15) and (19). The major weakness is that such strong alteration does not correspond to the extensive delocalization characteristic of conjugated polymers.

The number of 1A_g and 1B_u excitations for a chain of N dimers can readily be found for any combination of excited dimers. The singlet exciton for N dimers has $J=-1$ and leads to $N/2$ linear combinations with A and B symmetry for even N , or to $(N-1)/2$ states of A symmetry and $(N+1)/2$ states of B symmetry for odd N . The $J=1$ dimer state at E_a also gives $N/2$ states with A and B symmetry for even N , but has $(N+1)/2$ states of A symmetry and $(N-1)/2$ states of B symmetry for odd N . A similar analysis holds for constructing states with composite excitations. There are $N-1$ singlets with adjacent triplets, all with $J=1$, that form $(N-1)/2$ states of A and B symmetry for odd N , while even N leads to $N/2$ states A , $(N-2)/2$ states B . CT states again yield both $J=1$ and -1 . Adjacent D^+D^- are most important for the Ohno potential, while all $|CT,r\rangle$ contribute in Hubbard models. Crystal states based on three or more triplets, on CT states with excited dimers, or on $CT+T$ or other composite excitations can always be decomposed into A and B singlets of a chain.

¹*Molecular Nonlinear Optics: Materials, Physics, and Devices*, edited by J. Zyss (Academic, Orlando, FL, 1994); D. S. Chemla and J. Zyss, *Nonlinear Optical Properties of Organic Molecules and Crystals* (Academic, New York, 1987), Vols. 1 and 2.

²For recent work, see *Proceedings of the International Conference on the Science and Technology of Synthetic Metals, Tübingen, Germany, 1990* [Synth. Met. **41-43** (1991)]; *Proceedings of the International Conference on the Science and Technology of Synthetic Metals, Göteborg, Sweden, 1992* [Synth. Met. **55-57** (1993)].

³*Organic Electroluminescence*, edited by D. D. C. Bradley and

T. Tsutsui (Cambridge University Press, Cambridge, England, in press).

⁴A. J. Heeger, S. Kivelson, J. R. Schrieffer, and W. P. Su, *Rev. Mod. Phys.* **60**, 81 (1988).

⁵*Handbook of Conducting Polymers*, edited by T. A. Skotheim (Dekker, New York, 1988), Vols. 1 and 2.

⁶C. Halvorson, T. W. Hagler, D. Moses, Y. Cao, and A. J. Heeger, *Chem. Phys. Lett.* **200**, 364 (1992).

⁷Z. G. Soos and G. W. Hayden, in *Electroresponsive Molecular and Polymeric Systems*, edited by T. A. Skotheim (Dekker, New York, 1988), p. 197.

⁸R.G. Kepler and Z. G. Soos, in *Relaxation in Polymers*, edited

- by T. Kobayashi (World Scientific, Singapore, 1994), p. 100.
- ⁹P. W. Langhoff, S. T. Epstein, and M. Karplus, *Rev. Mod. Phys.* **44**, 602 (1972).
- ¹⁰Z. G. Soos, D. S. Galvão, and S. Etemad, *Adv. Mater.* **6**, 280 (1994).
- ¹¹Z. G. Soos, S. Ramasesha, and D. S. Galvão, *Phys. Rev. Lett.* **71**, 1609 (1993).
- ¹²D. Baeriswyl, D. K. Campbell, and S. Mazumdar, in *Conducting Polymers*, edited by H. Kiess, Springer Series in Solid-State Sciences Vol. 102 (Springer-Verlag, Heidelberg, 1992), p. 7.
- ¹³M. Pope and C. E. Swenberg, *Electronic Processes in Organic Crystals* (Clarendon, Oxford, 1982) provides a comprehensive introduction.
- ¹⁴N. F. Mott, *Proc. R. Soc. London* **62**, 416 (1949); *Rev. Mod. Phys.* **40**, 677 (1968); *Metal-Insulator Transitions* (Taylor & Francis, London, 1974).
- ¹⁵S. Abe, J. Yu, and W. P. Su, *Phys. Rev. B* **45**, 8264 (1992).
- ¹⁶S. Abe, *J. Phys. Soc. Jpn.* **58**, 62 (1989); in *Relaxation in Polymers* (Ref. 8), p. 215.
- ¹⁷F. B. Gallagher and F. C. Spano, *Phys. Rev. B* **50**, 5370 (1994).
- ¹⁸P. Tavan and K. Schulten, *Phys. Rev. B* **36**, 4337 (1987).
- ¹⁹J. R. Heflin, K. Y. Wong, O. Zamani-Khamiri, and A. F. Garito, *Phys. Rev. B* **38**, 1573 (1988).
- ²⁰A. Szabo and N. S. Ostlund, *Modern Quantum Chemistry: An Introduction to Advanced Electronic Structure Theory* (MacMillan, New York, 1982), p. 261ff.
- ²¹Z. G. Soos and D. J. Klein, in *Molecular Association*, edited by R. Foster (Academic, New York, 1975), Vol. 1, Chap. 1.
- ²²F. C. Zhang and T. M. Rice, *Phys. Rev. B* **37**, 3759 (1988); M. Sigrist, T. M. Rice, and F. C. Zhang, *ibid.* **49**, 12058 (1994).
- ²³W. A. Seitz and D. J. Klein, *Phys. Rev. B* **9**, 2159 (1974); **8**, 2236 (1973).
- ²⁴D. Guo and S. Mazumdar, *J. Chem. Phys.* **97**, 2170 (1992); P. C. M. McWilliams, Z. G. Soos, and G. W. Hayden, *ibid.* **97**, 2172 (1992).
- ²⁵Z. G. Soos and G. W. Hayden, *Chem. Phys.* **143**, 199 (1990).
- ²⁶P. C. M. McWilliams, G. W. Hayden, and Z. G. Soos, *Phys. Rev. B* **43**, 9777 (1991); S. Etemad and Z. G. Soos, in *Spectroscopy of Advanced Materials*, edited by R. J. H. Clark and R. E. Hester (Wiley, New York, 1991), Chap. 2.
- ²⁷Z. G. Soos and S. Ramasesha, *Phys. Rev. B* **29**, 5410 (1984).
- ²⁸Z. G. Soos and S. Ramasesha, in *Valence Bond Theory and Chemical Structure*, edited by D. J. Klein and J. Trinajstić (Elsevier, Amsterdam, 1990), p. 81.
- ²⁹Z. G. Soos and S. Ramasesha, *J. Chem. Phys.* **90**, 1067 (1989).
- ³⁰G. P. Agrawal, C. Cojan, and C. Flytzanis, *Phys. Rev. B* **17**, 776 (1978).
- ³¹L. Salem, *The Molecular Orbital Theory of Conjugated Systems* (Benjamin, New York, 1966).
- ³²A. D. McLachlan, *Mol. Phys.* **2**, 276 (1959).
- ³³O. J. Heilmann and E. H. Lieb, *Trans. N.Y. Acad. Sci.* **33**, 116 (1971); S. R. Bondeson and Z. G. Soos, *J. Chem. Phys.* **71**, 380 (1980).
- ³⁴P. C. M. McWilliams and Z. G. Soos, *J. Chem. Phys.* **95**, 2127 (1991).
- ³⁵Z. G. Soos, G. W. Hayden, P. C. M. McWilliams, and S. Etemad, *J. Chem. Phys.* **93**, 7439 (1990).
- ³⁶K. Ohno, *Theor. Chim. Acta* **2**, 219 (1964).
- ³⁷R. G. Kepler and Z. G. Soos, *Phys. Rev. B* **43**, 12530 (1991).
- ³⁸Z. G. Soos, S. Ramasesha, D. S. Galvão, and S. Etemad, *Phys. Rev. B* **47**, 1742 (1993); S. Ramasesha and Z. G. Soos, *J. Chem. Phys.* **98**, 4015 (1993).
- ³⁹Z. G. Soos, S. Kuwajima, and J. E. Mihalick, *Phys. Rev. B* **32**, 3124 (1985).
- ⁴⁰F. C. Spano and Z. G. Soos, *J. Chem. Phys.* **99**, 9265 (1993).
- ⁴¹E. H. Lieb and F. Y. Wu, *Phys. Rev. Lett.* **20**, 1445 (1968).
- ⁴²A. A. Ovchinnikov, *Zh. Eksp. Theor. Fiz.* **57**, 2137 (1969) [*Sov. Phys. JETP* **30**, 1100 (1970)].
- ⁴³S. Mazumdar and Z. G. Soos, *Phys. Rev. B* **23**, 2810 (1981).
- ⁴⁴D. Yaron and R. Silbey, *Phys. Rev. B* **45**, 11655 (1992); F. C. Spano, *Chem. Phys. Lett.* **211**, 491 (1993).
- ⁴⁵Z. G. Soos, R. G. Kepler, and S. Etemad, in *Organic Electroluminescence* (Ref. 3).
- ⁴⁶Z. G. Soos, S. Etemad, D. S. Galvão, and S. Ramasesha, *Chem. Phys. Lett.* **194**, 341 (1992).
- ⁴⁷Z. G. Soos and D. S. Galvão, *J. Phys. Chem.* **98**, 1029 (1994).
- ⁴⁸R. Pariser and R. G. Parr, *J. Chem. Phys.* **21**, 767 (1953); J. A. Pople, *Trans. Farad. Soc.* **42**, 1375 (1953).
- ⁴⁹K. Schulten, I. Ohmine, and M. Karplus, *J. Chem. Phys.* **64**, 4422 (1976); B. Roos and P. N. Skancke, *Acta Chem. Scand.* **21**, 233 (1967).
- ⁵⁰S. Ramasesha, D. S. Galvão, and Z. G. Soos, *J. Phys. Chem.* **97**, 2823 (1993).
- ⁵¹Z. G. Soos, D. S. Galvão, S. Etemad, and R. G. Kepler, in *Electrical, Optical, and Magnetic Properties of Organic Solid State Materials*, edited by A. F. Garito, A. K.-Y. Jen, L. R. Dalton, and C. Lee, MRS Symposia Proceedings No. 328 (Materials Research Society, Pittsburgh, 1994), p. 383.
- ⁵²C. Halvorson and A. J. Heeger, *Chem. Phys. Lett.* **216**, 488 (1993).
- ⁵³B. Lawrence, W. E. Torruellas, M. Cha, M. L. Sundheimer, G. I. Stegeman, J. Meth, S. Etemad, and G. L. Baker, *Phys. Rev. Lett.* **73**, 597 (1994).
- ⁵⁴C. J. Baker, O. M. Gelsen, and D. D. C. Bradley, *Chem. Phys. Lett.* **210**, 127 (1993).
- ⁵⁵Z. Shuai and J. L. Brédas, *Phys. Rev. B* **44**, 5962 (1991); X. Sun, Z. Shuai, R. Fu, K. Nasu, X. S. Li, D. L. Lin, and T. F. George, *J. Phys. Condens. Matter* **2**, 9713 (1990).
- ⁵⁶S. N. Dixit, D. Guo, and S. Mazumdar, *Phys. Rev. B* **43**, 6781 (1991).
- ⁵⁷D. Guo, S. Mazumdar, and S. N. Dixit, *Synth. Met.* **49**, 1 (1992); S. Mazumdar, D. Guo, and S. N. Dixit, *J. Chem. Phys.* **96**, 6862 (1996).
- ⁵⁸D. Guo, S. Mazumdar, and S. N. Dixit, *Nonlinear Opt.* **6**, 337 (1994).
- ⁵⁹F. Guo, D. Guo, and S. Mazumdar, *Phys. Rev. B* **49**, 10102 (1994).
- ⁶⁰Z. G. Soos, P. C. M. McWilliams, and G. W. Hayden, *Chem. Phys. Lett.* **171**, 14 (1990).
- ⁶¹B. E. Kohler, C. Spangler, and C. Westerfield, *J. Chem. Phys.* **89**, 5422 (1988); B. S. Hudson, B. E. Kohler, and K. Schulten, in *Excited States*, edited by E. Lim (Academic, New York, 1982), Vol. 6, Chap. 1.
- ⁶²Z. G. Soos and D. Mukhopadhyay, *J. Chem. Phys.* **101**, 5515 (1994).
- ⁶³L. Sebastian and G. Weiser, *Phys. Rev. Lett.* **46**, 1156 (1981); *Chem. Phys.* **62**, 447 (1981); G. Weiser, *Phys. Rev. B* **45**, 14076 (1991).
- ⁶⁴J. R. G. Thorne, S. T. Repinec, S. A. Abrash, J. M. Zeigler, and R. M. Hochstrasser, *Chem. Phys.* **146**, 315 (1990); J. R. G. Thorne, in *Relaxation in Polymers* (Ref. 8), p. 80.
- ⁶⁵T. Hasegawa, Y. Iwasa, H. Sunamura, T. Koda, Y. Tokura, H. Tachibana, M. Matsumoto, and S. Abe, *Phys. Rev. Lett.* **69**, 668 (1992).